5-2016

Manipulating Cardiovascular Cellular Interactions and Mechanics: A Multidimensional and Multimodal Approach

Aesha Yogesh Desai
Clemson University, adesai@g.clemson.edu

MANIPULATING CARDIOVASCULAR CELLULAR INTERACTIONS AND MECHANICS: A MULTIDIMENSIONAL AND MULTIMODAL APPROACH

A Dissertation
Presented to
the Graduate School of
Clemson University

In Partial Fulfillment
of the Requirements for the Degree
Doctor of Philosophy
Bioengineering

---

by
Aesha Yogesh Desai
May 2016

Accepted by:
Dr. Delphine Dean, Committee Chair
Dr. Agneta Simionescu
Dr. Jeremy Mercuri
Dr. Bruce Gao

ABSTRACT

The goal of this dissertation is to better understand cellular mechanics across length scales for the development of computational models of tissue behavior. To this end, we had two major approaches, multidimensional and multimodal. Firstly, to use a model that better mimics *in vivo* like cellular environment, microtissue (spheroid) cell culture system was used to study cell mechanics. Secondly, a novel technique was designed to study single cell mechanics in multiple dimensions.

Cell mechanical properties are directly related to the composition and organization of the cytoskeleton, which is physically coupled to neighboring cells through adherens junctions and to extracellular matrix through focal adhesion complexes. As such, we hypothesize that the variations in cellular interactions affects cell mechanics. To test our hypothesis, cardiomyocytes and vascular smooth muscle microtissues were cultured under several conditions that limited the cell-cell and cell-matrix interactions. Cell interactions facilitated by integrin β1, connexin 43, and N-cadherin was inhibited and their effect on cell stiffness was characterized by atomic force microscopy (AFM).

Currently, there does not exist a single technique that can measure mechanics of a single cell in two different dimensions. To address this gap, we designed a novel set up that combines two different single cell mechanics measurement techniques, AFM and carbon fiber. This combination allows for characterization of mechanical properties of single cells in multiple dimensions.

The results of these studies provide insights from a basic science perspective. The results provide information regarding cell mechanics in multiple dimensions at both

single cell as well microtissue level. The ultimate fulfillment of this work would be its incorporation into a multiscale model, leading to the ability to tie macro- scale behaviors to nano- scale phenomenon. Such models may help to better understand tissue behavior and further our understanding of the etiology of many diseases.

DEDICATION

I dedicate this work to my incredible family. To my parents, for emphasizing the value of education; supporting and encouraging me in letting me follow my dreams. Mum and dad, I would not be where I am today if it were not for your unconditional love and sacrifices you have made so I can pursue my college education in the USA. Daddy, it is in you that I find my strength and patience, and mum, my curiosity to 'why's and how's' surely nurtures from you. To my husband Keyur, for always being by my side and; sharing the challenges, uncertainties and sacrifices in the journey to dissertation.

ACKNOWLEDGMENTS

First and foremost, I express my greatest appreciation to my advisor, Dr.Delphine Dean. Her guidance, support and encouragement have been paramount in completing my dissertation. I will always be thankful to her for all the wonderful opportunities, from conferences to study abroad, that she has given me over the years that has helped me grow professionally. She has been a great inspiration, both academically and personally. Dr.Dean, your encouraging words, 'no panic, you will be fine' have definitely helped me see the light when I saw no hopes. Thank you for being an excellent role model, I have been fortunate to have the opportunity to work under your guidance.

I would also like to acknowledge Prof. Peter Kohl for giving me the opportunity to work in his laboratory at Imperial College London. Working under his tutelage for six months has been a great learning experience and his passion for science has been truly inspiring. I like to thank all the wonderful member of Prof. Kohl's lab for making my time in London memorable especially Dr.Remi Peyronnet for teaching me carbon fiber technique and helping me with all the experiments.

I would also like to thank all my committee members Dr. Agneta Simionescu, Dr. Jeremy Mercuri, and Dr. Bruce Gao for their time and feedback, which has helped me guide my research. Additionally, I would like to thank the laboratories of Dr. Bruce Gao and Dr. Martine LaBerge for harvesting the cells used in this work.

In addition, I would like to thank Dr. Sandra Deitch whose doctoral research laid the foundation for my own. I would also like to extend special thank you to Nadia Ayad, Dr.Jorge Rodriguez, Dr. Ruikai Chen, and all the other past and present members of the

Multiscale Bioelectromechancs Lab who have provided assistance with AFM expertise, cell culture and day-to-day lab work. Special shout out to the wonderful staff members of the Department of Bioengineering, Maria Torres and Melissa McCullough for greeting with the biggest cheerful smile and answering all the questions with immense patience. I take this opportunity to thank my prized friends, especially Tanzeel Kadiani for being there through thick and thin.

Finally I would like to acknowledge the financial support provided by the following grants: NIH P20 RR-016461 (to DD), NIH K25 HL092228 (to DD), NSF CAREER CBET 1254609 (to DD), ERC Advanced Grant CardioNECT (to PK).

TABLE OF CONTENTS

page

Table of Contents (Continued)

page

LIST OF TABLES

page

LIST OF FIGURES

page

List of figures (continued)

page

CHAPTER ONE

INTRODUCTION

1.1 Motivation

Cells in the body undergo mechanical stress every day. These stresses are particularly enhanced during injury or disease, such as atherosclerosis or myocardial infarction. Designs of successful treatments require characterization of effects of cellular interactions in cardiac as well as vascular cells. Various studies have indicated points of focal adhesions and adherens junctions as the principal sites of mechanical signalling in cell-cell and cell-matrix interactions respectively. So to better understand the importance of cellular junctions in its mechanics, first part of this study aims at understanding effects of blocking cell-cell and cell-matrix interactions on vascular smooth muscle cells and cardiomyocyte cellular microtissues. In order to have a better representation of *in vivo* like environment, studies were performed on scaffold free 3D culture system of cellular microtissues (spheroids) as they are known to mimic cellular microenvironment compared to 2D adherent culture.

Second part of this projects aims at characterizing multidimensional mechanics on a single cell by multiple modes. Muscle cells are known to generate active and passive forces both radially and axially as they contract. But, currently there are no techniques known to us that can quantify this bidirectional mechanics simultaneously. So our goal was to develop a technique that will bridge this gap. Future goal of this project is to building a computational model that can predict mechanical properties of cells based of

their microenvironment. In future, we hope to have a model, which on refinement can be applied to study tissue mechanics and can be used to design better cell-based therapies for cardiovascular diseases.

1.2 Research aims

1.2.1 Aim 1: Determine effects of cellular interactions on mechanical properties of vascular smooth muscle cells (VSMC) in 3d culture

We hypothesize that the heterogeneity observed in cells from a single population may partly be due to cell-cell and cell-matrix interactions in a given cell sample. In order to mimic more *in vivo* like cellular environment this study involved used scaffold free three dimensional cellular microtissues (spheroid) model. Specific cellular junctions of N-cadherin and integrin β1 were blocked using specific antibodies and its effects on cell mechanics were accessed by performing atomic force microscopy cytoindentation studies on day 5 microtissues.

1.2.2 Aim 2: Determine effects of cellular interactions on mechanical properties of cardiomyocytes (CM) in 3d culture

We hypothesize that the heterogeneity observed in cells from a single population may partly be due to cell-cell and cell-matrix interactions in a given cell sample. In order to mimic more *in vivo* like cellular environment this study involved used scaffold free three dimensional cellular microtissues (spheroid) model. Specific cellular junctions of

N-cadherin and connexin 43 were blocked using specific antibodies and its effects on mechanical properties were assed using atomic force microscopy.

1.2.3 Aim 3: Characterize radial and axial mechanics simultaneously on an individual isolated cardiomyocyte

With this aim our goal was to design a technique that can quantify both axial and radial mechanics on a single cell simultaneously. To this end, we combined carbon fiber technique that can manipulate and measure axial cells with atomic force microscopy, which is commonly used to manipulate and measure radial mechanics.

1.3 Significance

Cardiovascular diseases are the number one cause of mortality in United States. However, in spite of its gravity, not enough work has been done to improve the time required to cure these diseases. There are a wide variety of cardiovascular diseases whose etiology are either known or suspected to be related to abnormal cell mechanics, alteration of cellular mechanotransduction processes, or changes in tissue structure. But, research on how variations in cellular interactions affect its mechanics is still limited. Also, not enough information is available about multidirectional forces experienced by cells.

This study represents first attempt at understanding effects of cell-cell and cell-matrix interactions at microtissue level. Through this study we also present a novel design that combines AFM and CF techniques to characterize active and passive forces and

mechanics on a single isolated cardiomyocyte simultaneously. The results of these studies provide insights from a basic science perspective about the effects of cellular microenvironment (cell-cell and cell-matrix interactions, loading and unloading) on its mechanics.

To better understand cell's mechanics, it is important to closely translate results from in vitro experiments into mathematical relationships for in silico models. We believe, insights available from this study at single cell and microtissue level regarding the mechanical properties of cells we well as their response to different mechanical stimuli can be potentially used to develop tissue to organ level computational models. Such models may help to gain information on complex physiological properties or conditions and better understand tissue behavior and disease progression.

CHAPTER TWO

CURRENT STATE OF KNOWLEDGE

1.4 Cardiomyocytes

Cardiomyocytes (CM) account for 30% of the total number of cells within the myocardium (1, 2). They are required to contract in unison in order to provide effective pump action that can ensure adequate blood perfusion of the various organs and tissues (3). Cardiac muscle cells or CM are distributed throughout the heart but pacemaker cells are the ones that determine the natural beating frequency of cardiac muscle (4). They have the ability to contract due to the presence of highly organized cytoskeleton. The cytoplasm of myocytes, is filled with myofibrils, which are contractile bundle of fibers composed of many functional units called sarcomeres (5). The ends of myofibrils are anchored to the sarcolemma and the transmission of forces developed by the contracting myofibrils is secured by highly specialized cell-cell junctions, the intercalated discs (6).

Different cardiac cells act coherently with each other through intracellular junctions (e.g. gap junctions) forming a three dimensional (3D) syncytium (7). Two different intercellular adhesive junctions are found in the intercalated discs: adherens junctions and desmosomes, which anchor actin cytoskeleton and intermediate filaments, respectively, at the plasma membrane of adjoining cells, thereby provide mechanical attachment between the cells, and support the structural and functional integrity of the tissues (8). Cardiac development is also regulated by the extracellular matrix, which forms a mesh of structural and signaling networks encapsulating and connecting the cells (9). The cellular responses observed in cardiomyopathies arise from the detection of

functional changes mediated primarily by ECM–sarcomere connections and collectively aim to maintain sufficient contractile force and prevent progression to heart failure (10). The responses of cardiomyocytes to systemic stress or genetic abnormalities are modulated by mechanosensitive mechanisms within the cardiomyocyte (11-13). A complex network of proteins that connects the sarcomere to the ECM forms the basis of the mechanotransduction. Changes in wall stress induce signaling pathways that are associated with the development of cardiac pathology (10).

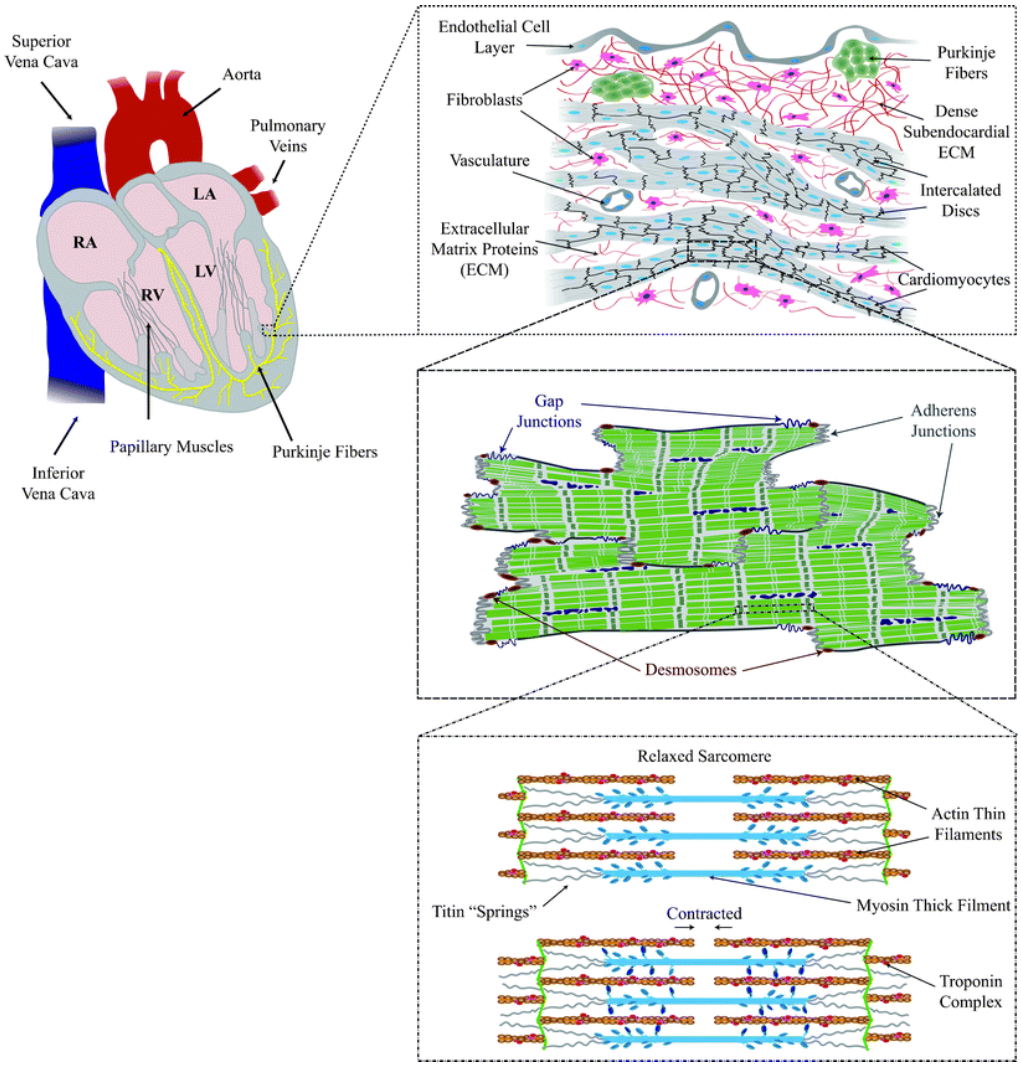

Figure 0.1: Schematic of heart, myocardium, cardiomyocytes, and sarcomeres (14).

1.5 Vascular smooth muscle cells

Vascular smooth muscle cells (VSMCs) are essential for good performance of the vasculature. The alter the lumen diameter thereby enabling blood vessels to maintain appropriate blood pressure by the process of contraction and relaxation. VSMCs also play important role in vessel remodeling in physiological conditions like exercise, pregnancy or after injury (15). Under these conditions, these cells synthesize large amounts of extracellular matrix components and increase proliferation and migration (16).

VSMCs express a wide range of phenotypes in vivo and in vitro cultures. The extremes of spectrum of their phenotypes have been termed ‘contractile’ and ‘synthetic’ by early investigators based on their primary functions of contraction and synthesis of extracellular matrix proteins (17). The contractile state is what is considered to be the primary state of VSMC in the normal adult aorta, while the synthetic phenotypes are seen in vivo during development and in response to injury followed by tissue repair (17). Pathologies such as atherosclerosis, hypertension, and diabetes dramatically affect the phenotype of the VSMC and the alteration of VSMC phenotype contributes to these disease states (15). During repair of vascular injury, dedifferentiated VSMCs participate in the formation of neointima by decreasing the expression of contractile proteins and increasing proliferation, migration, and matrix protein synthesis (18).

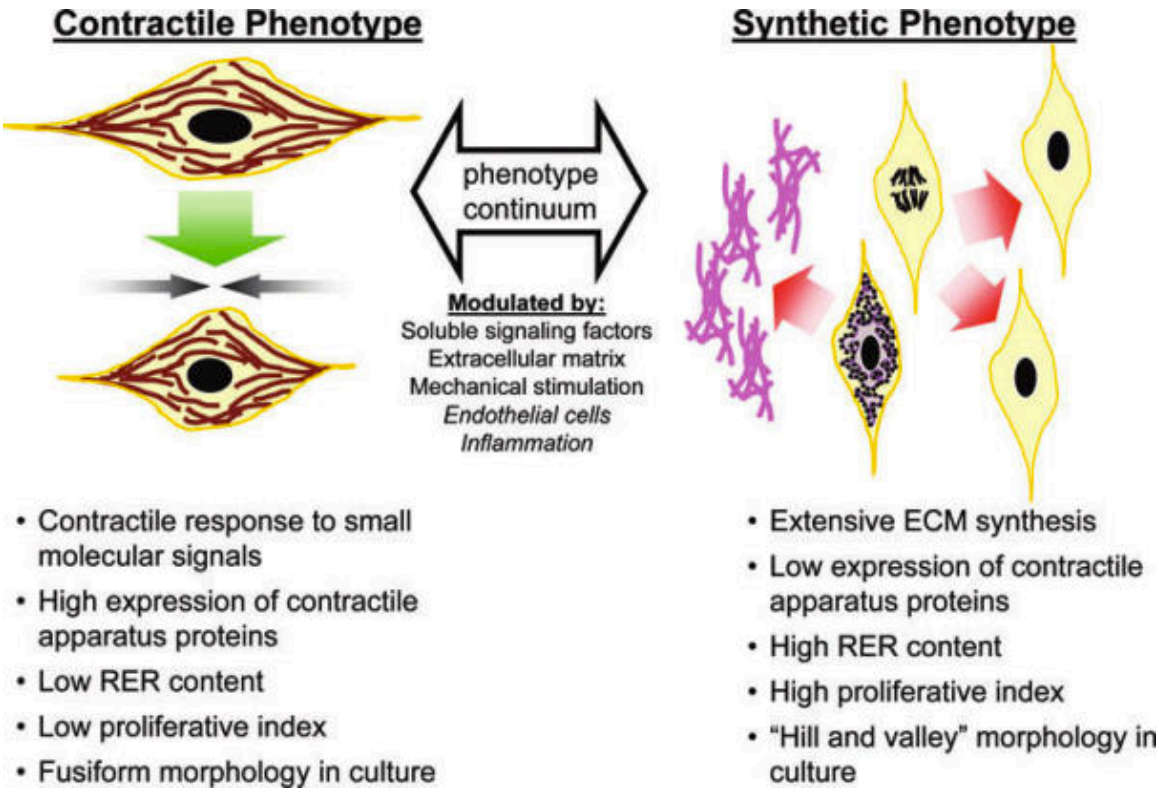

Figure 0.2: Summary of characteristics of SMC phenotypes, which vary along a continuum from synthetic and proliferative to contractile and quiescent. The position along this continuum is modulated by a variety of extracellular signals. ECM, extracellular matrix; RER, rough endoplasmic reticulum; SMC, smooth muscle cell (19).

1.6 2D Vs. 3D cell culture

Since the advent of routine cell culture more than forty-five years ago, the most common cell culture approach has been two dimensional (2D) on cell culture polystyrene or glass surface (20). Thousands of publications from cancer drug screening to developmental biology have relied on 2D adherent cell cultures (21). This approach provides a well-controlled, homogeneous environment that sustains cell proliferation for most cell types (22). However, 2D culture is far too simplistic and overlooks many parameters important for tissue physiology including mechanical cues, communication

between a cell and its matrix and communication between adjacent cells. For example, cells in natural environment not only adhere to each other but, are also embedded in an extracellular matrix (ECM) containing proteins like collagens, integrins, laminin, and fibronectin, which will affect cell shape (23), polarity (24), tension (25), differentiation (26) and help to organize communication between the cells (27). This results in significant differences in biological responses from cells in monolayer culture compared to those in organ or tissue *in vivo*.

Due to lack of 2D cell culture technologies to display tissue-like phenotypes, biologists are turning towards 3D cell culture options. Multicellular tumor spheroids (MCTS) have been used widely for over two decades and their utility is now receiving wider appreciation. MCTS reproduce the tumor microenvironment more accurately than 2D cultures (29-33), which have profound implications for tumor biology, particularly with respect to altered gene expression and sensitivity to chemotherapeutic agents (34). Hence, it is justified that 3D culture is clinically and biologically more relevant to *in vitro* models and it more closely mimics the native environment of the tissue. In addition, physical, chemical, and biological properties of a scaffold or vessel can be manipulated to manufacture unique materials to suit various purposes (35).

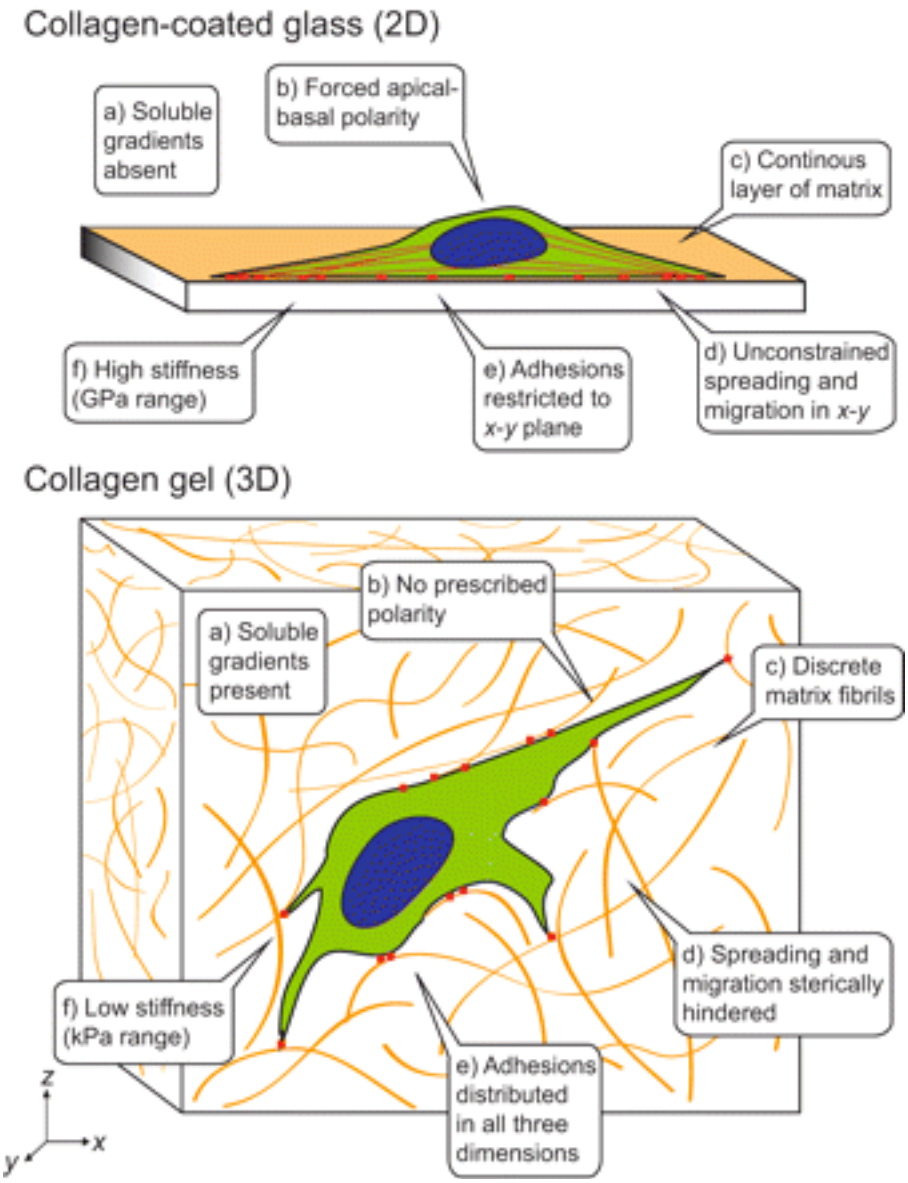

Figure 0.3: Differences in environmental cues in 2D vs. 3D cell culture. Adhesive, topographical, mechanical, and soluble cues. The cues encountered by a cell are strikingly different in adherent cell culture as compared to a typical 3D ECM (28).

1.7 3D Cell culture techniques

Two major approaches towards 3D cell culture are the ones with and without scaffolds. Seeding scaffolds, on which cells can re-establish their 3D structure, is

currently the standard technology. Scaffolds serve as substrate on which cell populations can attach and migrate, be implanted with combinations of specific cell types, as a cell delivery vehicle and be utilized as a drug carrier to activate specific cellular functions in a localized region (36). Scaffolds can be made out of natural substances or synthetic polymers. However, these matrices bear biological information and elicit biological response, which might differ from the response found in the natural environment (37). The inability of biomaterial scaffolds to functionally integrate into surrounding tissue is one of the major concerns to developing new biomaterials and tissue-engineering scaffolds (38). De-cellularized scaffolds serve as a great biocompatible material but with a risk of immunogenicity. Recent advancement to scaffold fabrication is electro spinning wherein very thin polymer fibers are spun to form web like scaffolds, which provide cells with more natural 3D environment (39).

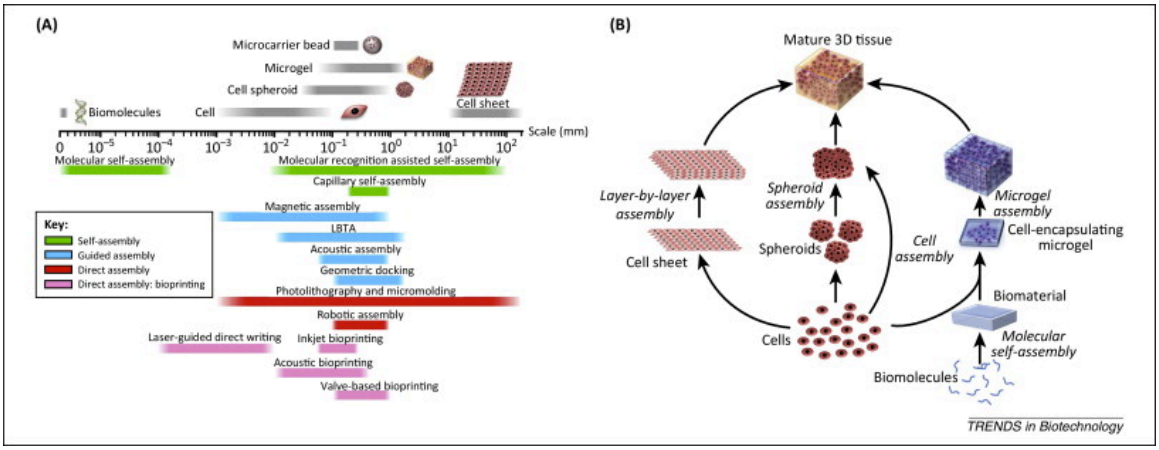

Figure 0.4: (A) Schematic of technologies for assembling building blocks at different scales. The size of each biological entity is shown above the scale axis, while the sample size that each assembly technology can manipulate is shown below the scale axis. (B) Schematic of multiscale assembly strategies from bottom to top for engineering 3D tissue constructs. The assembly strategies can follow paths starting with biomolecules or cells and can be integrated in the engineering of the final 3D tissue constructs (40).

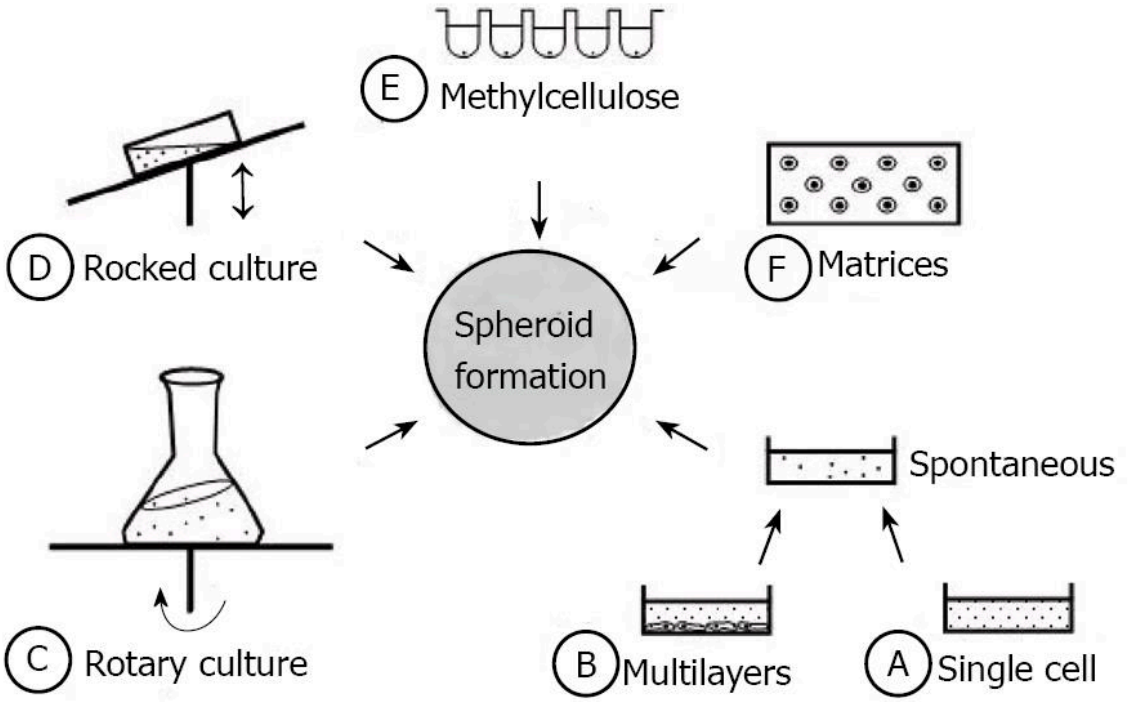

Figure 0.5: Different approaches to generation of scaffold free spheroids (41).

An alternative to scaffold based approach is scaffold free concept that involves formation of cellular aggregates called spheroids. Spheroid cultures are versatile and bio mimicry tool in many areas of (regenerative) medicine, basic science, and more application-oriented approaches (22). They are simple 3D models that form due to the tendency of cells to aggregate and can be generated from wide range of cell types (21). Cellular spheroids can be generated by multiple techniques such as, (i) gravity-enforced assembly of microspheres in hanging drop (24); (ii) cultivation in spinner flasks, static liquid overlay technique (LOT), gyratory shakers, roller bottles (42, 43); (iii) centrifugation (44); or non adhesive surfaces (45). Hanging drop technique is one of the oldest. It was invented by Harrison in 1907 and involves aggregation of cells in the

bottom of a drop after inverting a plate with drops of cell suspension (46). Spinner flasks enable spontaneous cell aggregation. In LOT, suspended cells are cultured on non-adherent substrates, and this causes cells to aggregate instead of adhering to the surface (47). For the purpose of this project, we will be focusing on investigating intercellular and cell matrix interaction on cell mechanics in a 3D environment and will be using hanging drop spheroid culture technique for the same.

1.8 References

1. Ehler E. Cardiac Cytoarchitecture: How to Maintain a Working Heart. Springer; 2015.

2. Iyer RK, Chui J, Radisic M. Spatiotemporal tracking of cells in tissue-engineered cardiac organoids. Journal of tissue engineering and regenerative medicine. 2009;3(3):196-207.

3. Woodcock EA, Matkovich SJ. Cardiomyocytes structure, function and associated pathologies. Int J Biochem Cell Biol. 2005;37(9):1746-51.

4. Mark GE, Strasser F. Pacemaker activity and mitosis in cultures of newborn rat heart ventricle cells. Exp Cell Res. 1966;44(2):217-33.

5. Gautel M. The sarcomeric cytoskeleton: who picks up the strain? Curr Opin Cell Biol. 2011;23(1):39-46.

6. Sheikh F, Ross RS, Chen J. Cell-cell connection to cardiac disease. Trends Cardiovasc Med. 2009;19(6):182-90.

7. Radisic M, Park H, Gerecht S, Cannizzaro C, Langer R, Vunjak-Novakovic G. Biomimetic approach to cardiac tissue engineering. Philos Trans R Soc Lond B Biol Sci. 2007 Aug 29;362(1484):1357-68.

8. Noorman M, van der Heyden, Marcel AG, van Veen TA, Cox MG, Hauer RN, de Bakker JM, et al. Cardiac cell–cell junctions in health and disease: electrical versus mechanical coupling. J Mol Cell Cardiol. 2009;47(1):23-31.

9. Kresh JY, Chopra A. Intercellular and extracellular mechanotransduction in cardiac myocytes. Pflügers Archiv-European Journal of Physiology. 2011;462(1):75-87.

10. Harvey PA, Leinwand LA. The cell biology of disease: cellular mechanisms of cardiomyopathy. J Cell Biol. 2011 Aug 8;194(3):355-65.

11. Molkentin JD, Dorn II GW. Cytoplasmic signaling pathways that regulate cardiac hypertrophy. Annu Rev Physiol. 2001;63(1):391-426.

12. Seidman J, Seidman C. The genetic basis for cardiomyopathy: from mutation identification to mechanistic paradigms. Cell. 2001;104(4):557-67.

13. Frey N, Olson E. Cardiac hypertrophy: the good, the bad, and the ugly. Annu Rev Physiol. 2003;65(1):45-79.

14. Simmons CS, Petzold BC, Pruitt BL. Microsystems for biomimetic stimulation of cardiac cells. Lab on a Chip. 2012;12(18):3235-48.

15. Owens GK, Kumar MS, Wamhoff BR. Molecular regulation of vascular smooth muscle cell differentiation in development and disease. Physiol Rev. 2004 Jul;84(3):767-801.

16. Rensen S, Doevendans P, Van Eys G. Regulation and characteristics of vascular smooth muscle cell phenotypic diversity. Netherlands Heart Journal. 2007;15(3):100-8.

17. Metz RP, Patterson JL, Wilson E. Vascular smooth muscle cells: isolation, culture, and characterization. Cardiovascular Development: Methods and Protocols. 2012:169-76.

18. Wang G, Jacquet L, Karamariti E, Xu Q. Origin and differentiation of vascular smooth muscle cells. J Physiol (Lond). 2015;593(14):3013-30.

19. Beamish JA, He P, Kottke-Marchant K, Marchant RE. Molecular regulation of contractile smooth muscle cell phenotype: implications for vascular tissue engineering. Tissue Engineering Part B: Reviews. 2010;16(5):467-91.

20. Wang F. Culture of animal cells: A manual of basic technique. In Vitro Cellular & Developmental Biology-Animal. 2006;42(5):169-.

21. Haycock JW. 3D cell culture: a review of current approaches and techniques. In: 3D Cell Culture. Springer; 2011. p. 1-15.

22. Fennema E, Rivron N, Rouwkema J, van Blitterswijk C, de Boer J. Spheroid culture as a tool for creating 3D complex tissues. Trends Biotechnol. 2013;31(2):108-15.

23. Goldmann WH. Mechanical aspects of cell shape regulation and signaling. Cell Biol Int. 2002;26(4):313-7.

24. Boudreau NJ. Organized living: from cell surfaces to basement membranes. Sci STKE. 2003 Aug 19;2003(196):pe34.

25. Tarone G, Hirsch E, Brancaccio M, De Acetis M, Barberis L, Balzac F, et al. Integrin function and regulation in development. Int J Dev Biol. 2000;44(6):725-32.

26. Bökel C, Brown NH. Integrins in development: moving on, responding to, and sticking to the extracellular matrix. Developmental cell. 2002;3(3):311-21.

27. Schenk S, Quaranta V. Tales from the crypt [ic] sites of the extracellular matrix. Trends Cell Biol. 2003;13(7):366-75.

28. Baker BM, Chen CS. Deconstructing the third dimension: how 3D culture microenvironments alter cellular cues. J Cell Sci. 2012 Jul 1;125(Pt 13):3015-24.

29. Sutherland RM. Cell and environment interactions in tumor microregions: the multicell spheroid model. Science. 1988 Apr 8;240(4849):177-84.

30. Mueller-Klieser W. Three-dimensional cell cultures: from molecular mechanisms to clinical applications. Am J Physiol. 1997 Oct;273(4 Pt 1):C1109-23.

31. Hamilton G. Multicellular spheroids as an in vitro tumor model. Cancer Lett. 1998;131(1):29-34.

32. KUNZ-SCHUGHART LA, Kreutz M, Knuechel R. Multicellular spheroids: a three-dimensional in vitro culture system to study tumour biology. Int J Exp Pathol. 1998;79(1):1-23.

33. Desoize B, Jardillier J. Multicellular resistance: a paradigm for clinical resistance? Crit Rev Oncol. 2000;36(2):193-207.

34. Dubessy C, Merlin J, Marchal C, Guillemin F. Spheroids in radiobiology and photodynamic therapy. Crit Rev Oncol. 2000;36(2):179-92.

35. Kawaguchi N, Machida M, Hatta K, Nakanishi T, Takagaki Y. Cell shape and cardiosphere differentiation: a revelation by proteomic profiling. Biochemistry research international. 2013;2013.

36. Shin H, Jo S, Mikos AG. Biomimetic materials for tissue engineering. Biomaterials. 2003;24(24):4353-64.

37. Hunziker EB. Articular cartilage repair: are the intrinsic biological constraints undermining this process insuperable? Osteoarthritis and Cartilage. 1999;7(1):15-28.

38. Vogel V, Baneyx G. The tissue engineering puzzle: a molecular perspective. Annu Rev Biomed Eng. 2003;5(1):441-63.

39. Khademhosseini A, Vacanti JP, Langer R. Progress in tissue engineering. Sci Am. 2009;300(5):64-71.

40. Guven S, Chen P, Inci F, Tasoglu S, Erkmen B, Demirci U. Multiscale assembly for tissue engineering and regenerative medicine. Trends Biotechnol. 2015;33(5):269-79.

41. van Zijl F, Mikulits W. Hepatospheres: Three dimensional cell cultures resemble physiological conditions of the liver. World J Hepatol. 2010 Jan 27;2(1):1-7.

42. Furukawa KS, Ushida T, Sakai Y, Suzuki M, Tanaka J, Tateishi T. Formation of human fibroblast aggregates (spheroids) by rotational culture. Cell Transplant. 2001;10(4-1):441-5.

43. Kelm JM, Timmins NE, Brown CJ, Fussenegger M, Nielsen LK. Method for generation of homogeneous multicellular tumor spheroids applicable to a wide variety of cell types. Biotechnol Bioeng. 2003;83(2):173-80.

44. Muraglia A, Corsi A, Riminucci M, Mastrogiacomo M, Cancedda R, Bianco P, et al. Formation of a chondro-osseous rudiment in micromass cultures of human bone-marrow stromal cells. J Cell Sci. 2003 Jul 15;116(Pt 14):2949-55.

45. Kale S, Biermann S, Edwards C, Tarnowski C, Morris M, Long MW. Three-dimensional cellular development is essential for ex vivo formation of human bone. Nat Biotechnol. 2000;18(9):954-8.

46. Harrison RG, Greenman M, Mall FP, Jackson C. Observations of the living developing nerve fiber. Anat Rec. 1907;1(5):116-28.

47. Yuhas JM, Li AP, Martinez AO, Ladman AJ. A simplified method for production and growth of multicellular tumor spheroids. Cancer Res. 1977 Oct;37(10):3639-43.

CHAPTER THREE

CELL MECHANICS: MANUPILATION AND MEASUREMENT

1.9 Cell mechanics and cellular junctions

Cells are integrated into tissues by several types of specialized intercellular junctions. Adherens junctions and desmosomes play an important role in integrating cytoskeletons of constituent cells into a mechanical syncytium, which is key to physiological tissue function (1-3). In developing organisms, mechanical forces generated by individual cells are transmitted and coordinated along intercellular junctions into tissue-level deformations that drive morphogenesis (4, 5). In adult organisms, intercellular junctions provide tissues with the strength necessary to withstand external forces, such as pulsatile shear stresses in blood vessels. In addition to providing mechanical strength, cellular junctions are dynamic, giving tissues fluidity by allowing neighbor exchange during development (6) and collective migration during wound healing (7). Complex signaling pathways regulate intercellular junctions, allowing single cells to organize into tissues or leading to tissue disaggregation (8).

The interactions of cardiac cells with the anisotropic structure of myocardium are paramount for regulation of the tissue properties such as synchronous contractility (9-12). Particularly, cellular organization and the orientation of the actin fibers, through contact guidance process, significantly influence the contractile force generated throughout the tissue (10-12). So, cardiovascular tissue remodeling in a diseased state (e.g. atherosclerosis, arrhythmia) can affect the extracellular matrix (ECM) composition (e.g. excessive collagen deposition) and consequently lead to poor cellular organization and

tissue contractility (13, 14). It has also been shown that junctional markers such as N-cadherin and connexin 43, which are responsible for mechanical and electrical signal propagation, are significantly influenced by cellular organization (15). Along with biophysical cues, ECM also provides biochemical cues such as various growth factors and ligands within the myocardium. It has been established that cells interact with the matrix through a combination of proteins collectively known as focal adhesion complex. Various transmembrane proteins such as vinculin and integrin β1 help in direct attachment of cell cytoskeleton to ECM and thus help in bidirectional transfer of biochemical and mechanical cues (16). For example, integrin β1 help in mechanotransduction between ECM and cardiomyocytes of cardiac fibroblasts (16, 17). They also assist in chemical signaling when any ligand binds to either intercellular receptor (inside-out signaling) or to extracellular receptor (outside-in signaling); initiating cascade of events. Stress applied through integrin specific adhesion sites increases cytoskeletal stiffening (18), activates second messenger formation (19), and induces tyrosine phosphorylation of the proteins anchored to the cytoskeleton (20). Integrin β1 are also characterized to play a definite role in myofibrillogenesis, cellular phenotypes and cell migration (17).

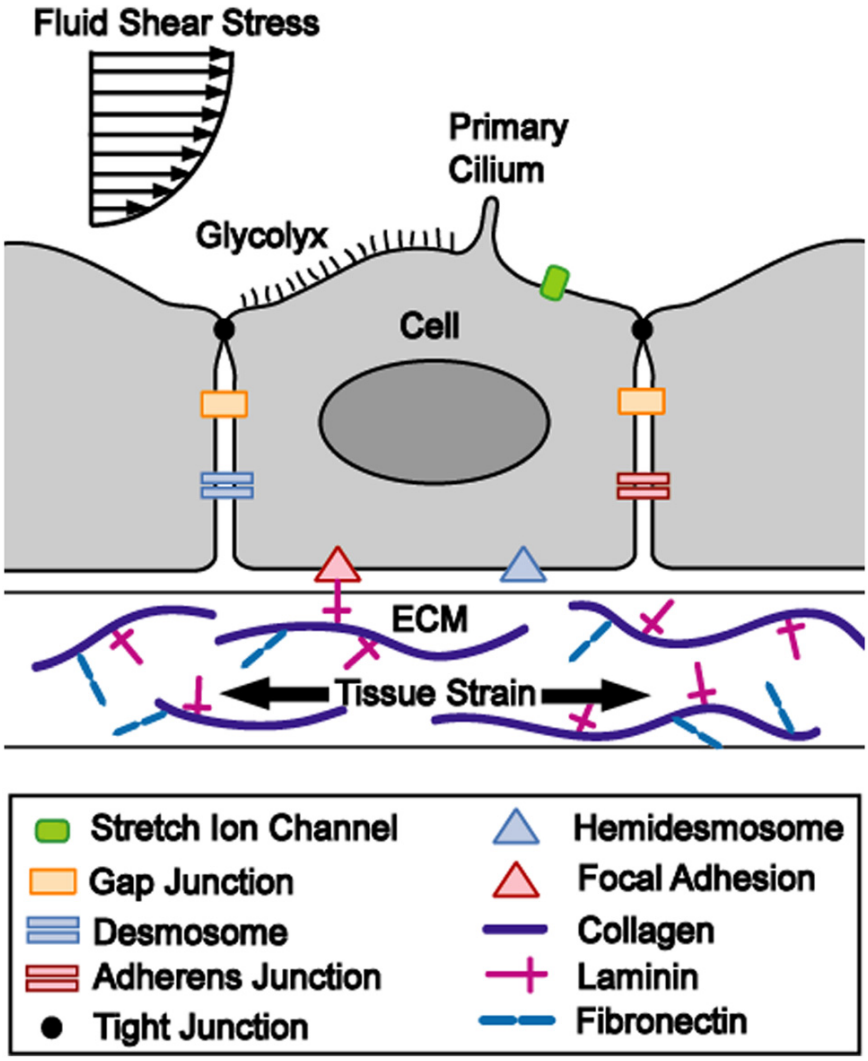

Figure 0.1: Mechanotransduction pathways and force sensing structures at cell-cell and cell-ECM junctions (21).

Like cell-ECM, cell-cell interactions also play a crucial role in maintaining the intercellular communication between cells. Homogeneous or heterogeneous cell types communicate intercellularly either through gap junctions or adherens (12). Gap junctions are intercellular proteins that allow the direct flow of molecules, solutes and ions from one cytoplasm to another in between the adjacent cells (22). In addition, gap junctions are

mainly responsible for electrical impulse propagation between the two couples cells. The most identified gap junctions in heart have been connexin 43, 45, and 40 (22, 23). Various studies have observed that connexin 43 gets expressed at either homogeneous cellular junction such as in between cardiomyocytes or and at heterogeneous cellular junctions between cardiomyocyte and cardiac fibroblast cells (23). Due to the presence of gap junction molecules, an electrical syncytium is established in between the myocardial cells, which thereby ensures synchronous contraction of the tissue within the myocardium (24).

1.10 Techniques to manipulate and measure cell mechanics

Measuring mechanical properties of any material, including cells requires application of some kind of force to it and record its deformation response. Forces can be applied in many modes, tension or compression; uniaxial or biaxial; bending, twisting, torsion, or shear. Techniques available to apply controlled deformation and forces on part of, or an entire cell (Figure **0**.**2**) (Table **0**.**1**). These techniques include but are not limited to magnetic bead cytometry (25-27), optical tweezers (28-30), cell stretchers (31-34), flow rheometry (33, 35, 36), and atomic force microscopy (AFM) (37). Along with variety of tools available to manipulate cell mechanics, a wide array of techniques have been developed that can measure the mechanical properties of cells on spatially accurate length scales (38). Techniques that can monitor the ability of a cell to generate forces and deform its environment are micro pillar arrays (39) and traction force microscopy (TFM) (40, 41).

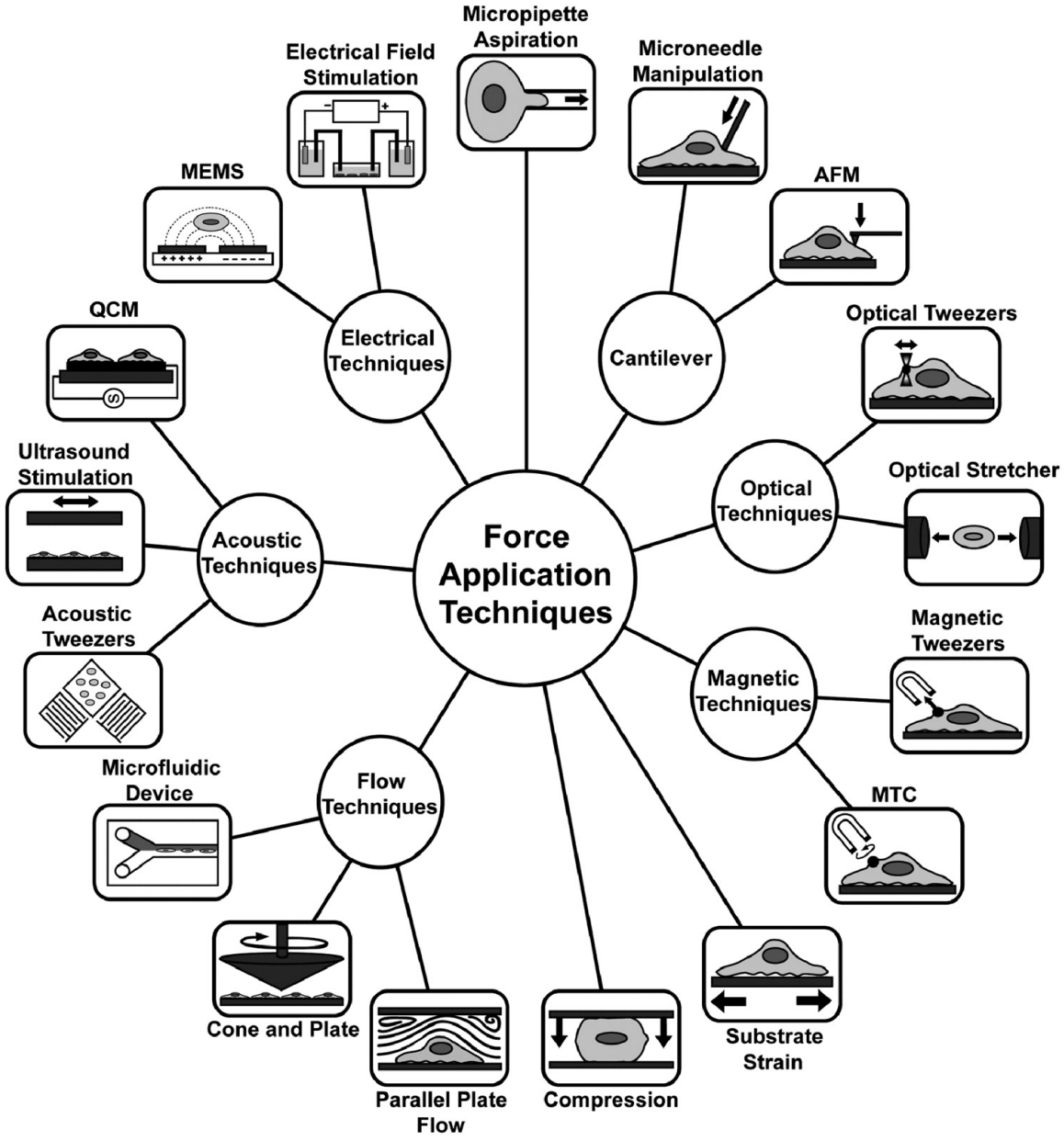

Figure 0.2: Various techniques used to apply force on cells (21).

Table 0.1: Summary of methods and techniques in cellular biomechanics (42)

Method	Principle	Range of forces that can be applied or detected
Atomic force microscopy (AFM)	Relative deformation of cantilever tip and substrate (cell) is used to estimate forces.	~10 pN $\leq \mathbf{F}_x \leq$?
Micropipette aspiration	Gentle suction is applied to micropipette attached to cell.	10–20 pN $\leq \mathbf{F}_x \leq$?
Stretching devices	Flexible membrane is attached to structures that enable membrane to be stretched	Qualitative-at least 25% from unstretched state
Carbon fiber (CF)-based systems	Carbon fibers are attached directly to a cell and controlled mechanically using feedback systems.	? $\leq \mathbf{F}_x \leq$ 5 μN
Magnetic tweezers/magnetic twisting cytometry	Magnetized ferromagnetic or superparamagnetic beads are moved by weaker directional magnetic fields/gradients.	2 pN $\leq \mathbf{F}_x \leq$ 50 nN
Optical tweezers	Dielectric beads of high refractive index are moved using laser beams.	~2 pN $\leq \mathbf{F}_x \leq$ 600 pN
MEMS in silicon	Movable parts are fabricated in silicon and various methods such as piezo actuation are used to move them.	0.5 nN $\leq \mathbf{F}_x \leq$ 1.5 μN
Flow chambers	Enclosed chambers with inlet and outlets for fluid flow are used to subject cells to fluid shear stress.	30 Pa $\leq P_x \leq$?
Elastic substratum method	Wrinkling patterns developed in artificial flexible sheets are used to infer cell traction forces.	Qualitative
Flexible sheets with embedded beads	Displacements of beads within flexible sheets are used to infer cell traction forces	140 nN $\leq \mathbf{F}_x \leq$?
Flexible sheets with micropatterned dots or grids	Deformation of grid or dot patterns from ideal is used to infer cell traction forces.	70 nN $\leq \mathbf{F}_x \leq$?
Array of vertical microcantilevers	Horizontal deflection of individual vertical microcantilevers is used to infer traction forces.	50 pN $\leq \mathbf{F}_x \leq$ 100 nN
Micromachined horizontal cantilever	Horizontal deflection of cantilever with attachment pad is used to infer traction force.	~2 nN $\leq \mathbf{F}_x \leq$ 100 nN

1.11 Atomic force microscopy (AFM)

The AFM is a high-resolution surface characterization technique that is been routinely used for imaging and mechanical characterization of a range of biological samples (37). AFM measurement uses a micron-sized tip/probe connected to a micro-fabricated cantilever beam to deform and interact with the sample. It can be used to probe surface topography as well as interaction forces with subnano-meter and pico-newton resolution (38). One of the most widespread uses of AFM in cell mechanics is for force spectroscopy to measure cellular elasticity and rheology. To measure the cell elasticity, the tip of AFM cantilever is pressed against the cell while the force and the imposed cellular deformation are monitored. Considering the tip geometry and using appropriate contact model, the elasticity of the cell can be computed from the measured force versus indentation data (43). The most commonly used model for interpreting the depression-force relationship is referred to as the Hertzian (44, 45) model and ssumes semi-infinite, linearly elastic, homogeneous substance. As the levels of force and deformation can be very accurately measured over time, AFM has been applied for a variety of rheological measurements. Using a feedback loop levels of stress and strain can be controlled over time, following indentation of the cell via the cantilever.

Cell biology and medicine are particularly interested in the capability of AFM to monitor changes in cell elasticity under different pharmacological and genetic perturbation (46, 47).

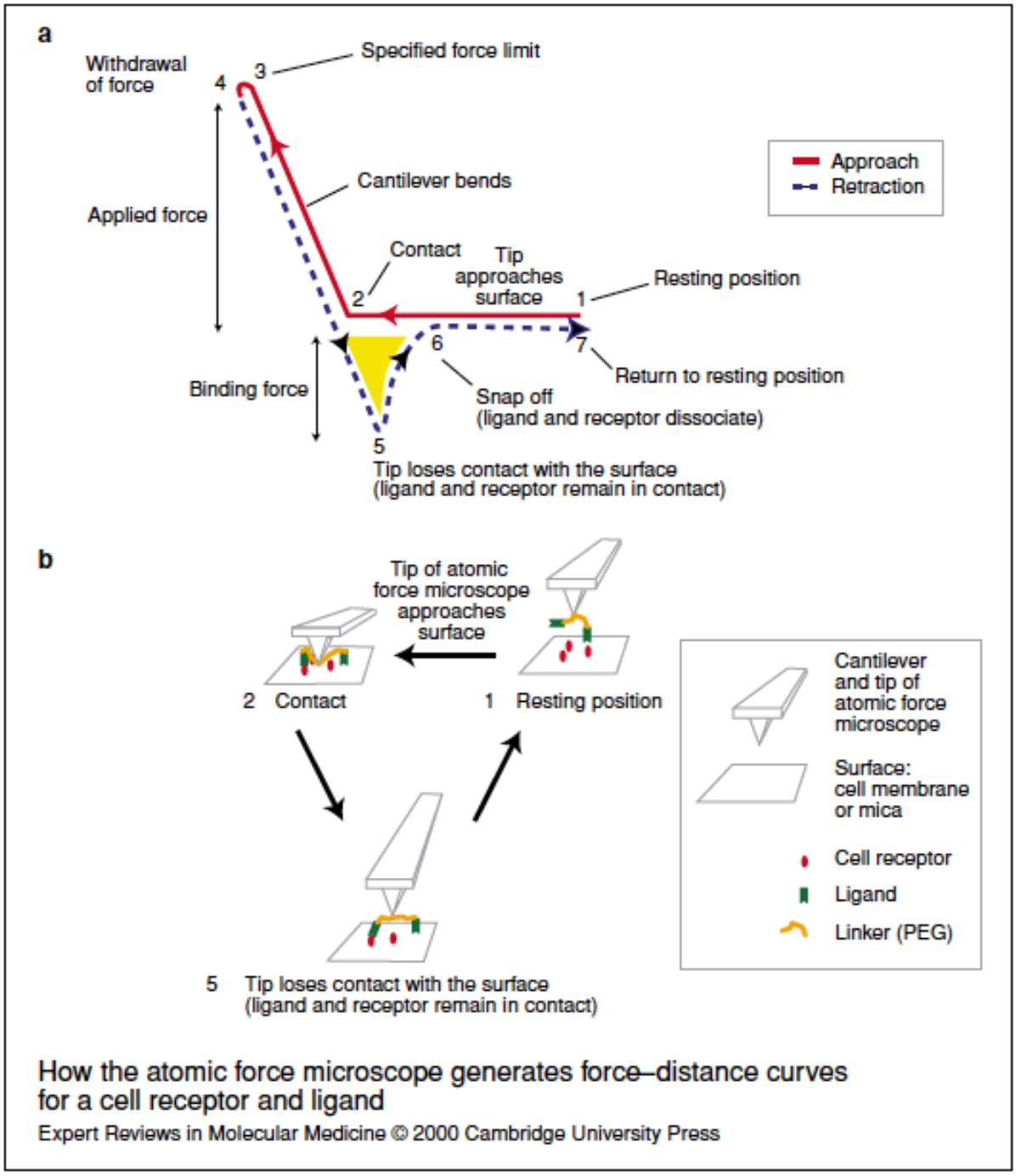

How the atomic force microscope generates force–distance curves for a cell receptor and ligand

Figure 0.3: Schematic representing how the atomic force microscope generates force-distance curves for a cell receptor and ligand (48).

1.12 Carbon fiber (CF) technique

This technique involves the use of carbon fibers mounted in glass capillaries attached to precise position control device with feedback control mechanism. CFs are attached to cells and used as a means to apply active forces and record forces generated by the cell. The image of CFs is projected through optics onto a photodiode array, which converts this into a usable signal for the feedback control system. The optical system is also connected to an image recording system and can be used to capture and record changed in the length of the cell (Figure **0**.**4**(A)) (42). This technique has the potential to be applied to variety of cell types but currently it is mainly used to investigate mechanics of single cardiac myocytes. Yasuda et al. (49) used this method to characterize mechanics of single rat cardiac myocyte under isometric and physiologically loaded conditions. Nishimura et al. (50) also performed similar studies by making modifications and improvements to the feedback control system used by Yasuda et al. Iribe et al. (51) made further modifications to this set up by introducing the use of bidirectional control instead of the single-sided control used by Yasuda et al. and Nishimura et al. which reduced sarcomere blurring (Figure **0**.**4**(B)). CF approach provides true, closed-loop mechanical control of a single cell, in which the compliance of the measurement system can be controlled independently of its displacement, thereby allowing exploration of cellular mechanics over the full range of forces, displacements, and velocities that are required to fully specify the parameters for an active, viscoelastic model of cellular mechanics (42).

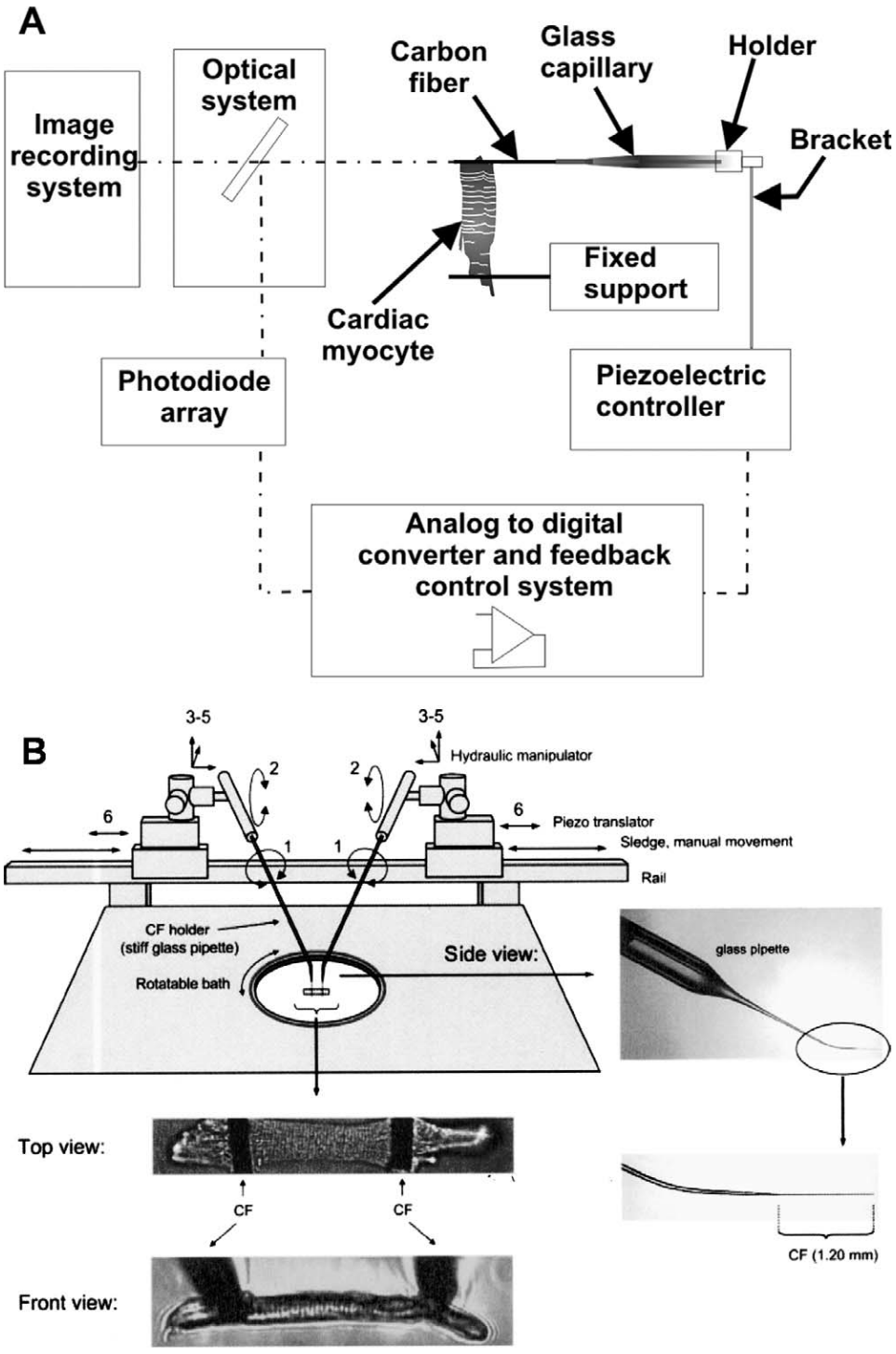

Figure 0.4: Schematic of carbon fiber (CF) set up. Active control of pairs CFs for studies of cardiomyocyte mechanics. A) Schematic showing the general principle of operation of the CF system used by Yasuda *et al*. (42, 49) B) Experimental set up and images of CFs attached to individual cardiac myocytes (from Iribe *et al*.) (42, 51).

1.13 References

1. Getsios S, Huen AC, Green KJ. Working out the strength and flexibility of desmosomes. Nature Reviews Molecular Cell Biology. 2004;5(4):271-81.

2. Green KJ, Simpson CL. Desmosomes: new perspectives on a classic. J Invest Dermatol. 2007;127(11):2499-515.

3. Harris TJ, Tepass U. Adherens junctions: from molecules to morphogenesis. Nature reviews Molecular cell biology. 2010;11(7):502-14.

4. Blanchard GB, Kabla AJ, Schultz NL, Butler LC, Sanson B, Gorfinkiel N, et al. Tissue tectonics: morphogenetic strain rates, cell shape change and intercalation. Nature methods. 2009;6(6):458-64.

5. Martin AC, Gelbart M, Fernandez-Gonzalez R, Kaschube M, Wieschaus EF. Integration of contractile forces during tissue invagination. J Cell Biol. 2010 Mar 8;188(5):735-49.

6. Ranft J, Basan M, Elgeti J, Joanny JF, Prost J, Julicher F. Fluidization of tissues by cell division and apoptosis. Proc Natl Acad Sci U S A. 2010 Dec 7;107(49):20863-8.

7. Poujade M, Grasland-Mongrain E, Hertzog A, Jouanneau J, Chavrier P, Ladoux B, et al. Collective migration of an epithelial monolayer in response to a model wound. Proc Natl Acad Sci U S A. 2007 Oct 9;104(41):15988-93.

8. Thiery JP, Sleeman JP. Complex networks orchestrate epithelial–mesenchymal transitions. Nature reviews Molecular cell biology. 2006;7(2):131-42.

9. Feinberg AW, Feigel A, Shevkoplyas SS, Sheehy S, Whitesides GM, Parker KK. Muscular thin films for building actuators and powering devices. Science. 2007 Sep 7;317(5843):1366-70.

10. Au HTH, Cui B, Chu ZE, Veres T, Radisic M. Cell culture chips for simultaneous application of topographical and electrical cues enhance phenotype of cardiomyocytes. Lab on a chip. 2009;9(4):564-75.

11. Au HTH, Cheng I, Chowdhury MF, Radisic M. Interactive effects of surface topography and pulsatile electrical field stimulation on orientation and elongation of fibroblasts and cardiomyocytes. Biomaterials. 2007;28(29):4277-93.

12. Zhang P, Su J, Mende U. Cross talk between cardiac myocytes and fibroblasts: from multiscale investigative approaches to mechanisms and functional consequences. Am J Physiol Heart Circ Physiol. 2012 Dec 15;303(12):H1385-96.

13. Biernacka A, Frangogiannis NG. Aging and Cardiac Fibrosis. Aging Dis. 2011 Apr;2(2):158-73.

14. Baig MK, Mahon N, McKenna WJ, Caforio AL, Bonow RO, Francis GS, et al. The pathophysiology of advanced heart failure. Am Heart J. 1998;135(6):S216-30.

15. Patel AA, Desai TA, Kumar S. Microtopographical assembly of cardiomyocytes. Integrative Biology. 2011;3(10):1011-9.

16. Samarel AM. Costameres, focal adhesions, and cardiomyocyte mechanotransduction. Am J Physiol Heart Circ Physiol. 2005 Dec;289(6):H2291-301.

17. Ross RS, Borg TK. Integrins and the myocardium. Circ Res. 2001 Jun 8;88(11):1112-9.

18. Wang N, Butler JP, Ingber DE. Mechanotransduction across the cell surface and through the cytoskeleton. Science. 1993 May 21;260(5111):1124-7.

19. McNamee HP, Ingber DE, Schwartz MA. Adhesion to fibronectin stimulates inositol lipid synthesis and enhances PDGF-induced inositol lipid breakdown. J Cell Biol. 1993 May;121(3):673-8.

20. Schmidt C, Pommerenke H, Durr F, Nebe B, Rychly J. Mechanical stressing of integrin receptors induces enhanced tyrosine phosphorylation of cytoskeletally anchored proteins. J Biol Chem. 1998 Feb 27;273(9):5081-5.

21. Rodriguez ML, McGarry PJ, Sniadecki NJ. Review on cell mechanics: experimental and modeling approaches. Appl Mech Rev. 2013;65(6):060801.

22. Souders CA, Bowers SL, Baudino TA. Cardiac fibroblast: the renaissance cell. Circ Res. 2009 Dec 4;105(12):1164-76.

23. Camelliti P, Borg TK, Kohl P. Structural and functional characterisation of cardiac fibroblasts. Cardiovasc Res. 2005 Jan 1;65(1):40-51.

24. Eckardt D, Theis M, Degen J, Ott T, Van Rijen H, Kirchhoff S, et al. Functional role of connexin43 gap junction channels in adult mouse heart assessed by inducible gene deletion. J Mol Cell Cardiol. 2004;36(1):101-10.

25. Wang N, Butler JP, Ingber DE. Mechanotransduction across the cell surface and through the cytoskeleton. Science. 1993 May 21;260(5111):1124-7.

26. Fabry B, Maksym GN, Butler JP, Glogauer M, Navajas D, Fredberg JJ. Scaling the microrheology of living cells. Phys Rev Lett. 2001;87(14):148102.

27. Deng L, Trepat X, Butler JP, Millet E, Morgan KG, Weitz DA, et al. Fast and slow dynamics of the cytoskeleton. Nature materials. 2006;5(8):636-40.

28. Balland M, Desprat N, Icard D, Féréol S, Asnacios A, Browaeys J, et al. Power laws in microrheology experiments on living cells: Comparative analysis and modeling. Physical Review E. 2006;74(2):021911.

29. Schmidt CE, Horwitz AF, Lauffenburger DA, Sheetz MP. Integrin-cytoskeletal interactions in migrating fibroblasts are dynamic, asymmetric, and regulated. J Cell Biol. 1993 Nov;123(4):977-91.

30. Henon S, Lenormand G, Richert A, Gallet F. A new determination of the shear modulus of the human erythrocyte membrane using optical tweezers. Biophys J. 1999;76(2):1145-51.

31. Krishnan R, Park CY, Lin Y, Mead J, Jaspers RT, Trepat X, et al. Reinforcement versus fluidization in cytoskeletal mechanoresponsiveness. PloS one. 2009;4(5):e5486.

32. Katsumi A, Milanini J, Kiosses WB, del Pozo MA, Kaunas R, Chien S, et al. Effects of cell tension on the small GTPase Rac. J Cell Biol. 2002 Jul 8;158(1):153-64.

33. Steward RL, Cheng C, Jonathan DY, Bellin RM, LeDuc PR. Mechanical stretch and shear flow induced reorganization and recruitment of fibronectin in fibroblasts. Scientific reports. 2011;1.

34. Harris AR, Bellis J, Khalilgharibi N, Wyatt T, Baum B, Kabla AJ, et al. Generating suspended cell monolayers for mechanobiological studies. Nature protocols. 2013;8(12):2516-30.

35. Lu H, Koo LY, Wang WM, Lauffenburger DA, Griffith LG, Jensen KF. Microfluidic shear devices for quantitative analysis of cell adhesion. Anal Chem. 2004;76(18):5257-64.

36. Gossett DR, Tse HT, Lee SA, Ying Y, Lindgren AG, Yang OO, et al. Hydrodynamic stretching of single cells for large population mechanical phenotyping. Proc Natl Acad Sci U S A. 2012 May 15;109(20):7630-5.

37. Müller DJ, Dufrene YF. Atomic force microscopy as a multifunctional molecular toolbox in nanobiotechnology. Nature nanotechnology. 2008;3(5):261-9.

38. Moeendarbary E, Harris AR. Cell mechanics: principles, practices, and prospects. Wiley Interdisciplinary Reviews: Systems Biology and Medicine. 2014;6(5):371-88.

39. Fu J, Wang Y, Yang MT, Desai RA, Yu X, Liu Z, et al. Mechanical regulation of cell function with geometrically modulated elastomeric substrates. Nature methods. 2010;7(9):733-6.

40. Munevar S, Wang Y, Dembo M. Traction force microscopy of migrating normal and H-ras transformed 3T3 fibroblasts. Biophys J. 2001;80(4):1744-57.

41. Legant WR, Miller JS, Blakely BL, Cohen DM, Genin GM, Chen CS. Measurement of mechanical tractions exerted by cells in three-dimensional matrices. Nature methods. 2010;7(12):969-71.

42. Addae-Mensah KA, Wikswo JP. Measurement techniques for cellular biomechanics in vitro. Exp Biol Med (Maywood). 2008 Jul;233(7):792-809.

43. Harris AR, Charras G. Experimental validation of atomic force microscopy-based cell elasticity measurements. Nanotechnology. 2011;22(34):345102.

44. Hertz H. Über die Berührung fester elastischer Körper. Journal für die reine und angewandte Mathematik. 1882;92:156-71.

45. Radmacher M, Fritz M, Hansma PK. Imaging soft samples with the atomic force microscope: gelatin in water and propanol. Biophys J. 1995 Jul;69(1):264-70.

46. Kunda P, Rodrigues NT, Moeendarbary E, Liu T, Ivetic A, Charras G, et al. PP1-mediated moesin dephosphorylation couples polar relaxation to mitotic exit. Current biology. 2012;22(3):231-6.

47. Moulding DA, Moeendarbary E, Valon L, Record J, Charras GT, Thrasher AJ. Excess F-actin mechanically impedes mitosis leading to cytokinesis failure in X-linked neutropenia by exceeding Aurora B kinase error correction capacity. Blood. 2012 Nov 1;120(18):3803-11.

48. Horton MA, Lehenkari PP, Charras GT, Nesbitt SA. New technologies in scanning probe microscopy for studying molecular interactions in cells. Expert reviews in molecular medicine. 2000;2(02):1-19.

49. Yasuda SI, Sugiura S, Kobayakawa N, Fujita H, Yamashita H, Katoh K, et al. A novel method to study contraction characteristics of a single cardiac myocyte using carbon fibers. Am J Physiol Heart Circ Physiol. 2001 Sep;281(3):H1442-6.

50. Nishimura S, Yasuda S, Katoh M, Yamada KP, Yamashita H, Saeki Y, et al. Single cell mechanics of rat cardiomyocytes under isometric, unloaded, and physiologically loaded conditions. Am J Physiol Heart Circ Physiol. 2004 Jul;287(1):H196-202.

51. Iribe G, Helmes M, Kohl P. Force-length relations in isolated intact cardiomyocytes subjected to dynamic changes in mechanical load. Am J Physiol Heart Circ Physiol. 2007 Mar;292(3):H1487-97.

CHAPTER FOUR

CHARACTERIZING EFFECTS OF BLOCKING CELLULAR INTERACTIONS ON MECHANICAL PROPERTIES OF CARDIOMYOCYTE AND VASCULAR SMOOTH MUSCLE CELL SPHEROIDS

1.14 Introduction

Mechanical properties of cells, especially stiffness of cells and their surrounding extracellular matrix are critical for many biological processes including cell growth, division, differentiation, motility, and tissue homeostasis (1, 2). Changes in cell mechanical properties are also often found to be closely associated with various disease conditions. Monitoring mechanical stiffness of living cells can therefore provide a way to monitor cell physiology, detect and diagnose diseases, and also evaluate the effectiveness of drug treatments (3, 4). Multiple methods have been developed over the years to measure cellular stiffness, elasticity. One of the most widely used methods to characterize mechanical properties of cells and tissues is atomic force microscopy (AFM) (5). It is a microindentation technique wherein an indenter with well-defines geometry is used to indent into cells.

Cells sense and respond to physical stimuli from the environment by the process called mechanotransduction. Various studies (6-9) have indicated points of focal adhesions and adherens junctions as the principal sites of mechanical signalling in cell-cell and cell-matrix interactions respectively. The interaction between cardiac cells with anisotropic structure of myocardium is crucial for the regulation of tissue properties such as synchronous contractility (10-13). Extracellular matrix provides biophysical and biochemical cues such as various growth factors and ligands within the myocardium.

Cells interact with the matrix through a combination of proteins called focal adhesion complex. Various transmembrane proteins like vinculin and integrin β1 help in direct attachment of cell cytoskeleton to ECM and help in bidirectional transfer of biochemical/mechanical signals (14). Cell-cell interactions mediated by either gap or adherens junctions also play an important role in maintaining intercellular communication between cells (13). Most commonly identified gap junctions in heart cells are connexin 43, 45, and 40 (15). Studies have shown that connexin 43 and 45 are expressed in cardiac cells at homogeneous (between cardiomyocytes) and heterogeneous (between cardiomyocytes and cardiac fibroblasts) cellular junctions (16). Cardiovascular cells are also known to communicate with each other intercellularly through adherens junctions, which are transmembrane proteins that interconnect the actin/intermediate filaments of adjacent cells (13). These proteins are known to mechanically couple the cells and participate in myofibril organization along with other proteins such as integrin β1 (17).

Realizing the importance of cellular interactions, the goal of our study was to understand the effects of blocking cell-cell and cell-matrix interactions, particularly integrin β1 and N-cadherin interactions in vascular smooth muscle cells (VSMCs) and integrin β1 and connexin 43 interactions in cardiomyocytes (CMs) on the mechanical properties (stiffness) of cells. In order to have a better representation of *in vivo* like environment, studies were performed on scaffold free 3D culture system of cellular microtissues (spheroids).

Our study involves the use of 3D cell culture approach that will enable us to better mimic the native tissue form. Traditional 2D culture have not been able to replicate biological characteristics due to differences in cellular interactions among cells on flat plates as compared to *in vivo* tissues (18, 19). Various techniques such as filter inserts, polymer scaffolds, hydrogels, microfluidic chips, etc. have been developed to overcome this limitation (20-24). Among these methods, cell aggregate or spheroid culture method have been widely used for practical applications such as drug development and stem cell differentiation as they mimic tissue characteristics well (25, 26). Various techniques have been developed over the years to form spheroids such as hanging drop, spinner flasks, non-adherent surfaces, micro-fabricated scaffolds, microfluidic chips, stimulus-responsive hydrogels and magnetic levitation (27-31). Our study involves use of hanging drop technique, as it is a relatively easy approach not requiring any special skill sets or equipment.

1.15 Materials and methods

Cell isolation and culture

Primary cardiomyocytes (CMs) isolated from neonatal (3 day) rat hearts were used in his used. To isolate the cells, heart was removed, minced and subjected to collagenase dissociation by following established protocol (32). Aortic smooth muscle cells (VSMCs) were isolated from week 12 Sprague-Dawley rats as outlined in appendix A. The isolated cells were allowed to culture in T75 flasks under standard conditions (37°C, 5% CO_2) supplemented with media containing DMEM (Dulbeccos Modified Eagles Medium) (Hyclone, Fisher scientific), 10% fetal bovine serum (FBS)

(Atlanta Biologicals), and 1% antibiotic/antimycotic solution (Gibco life technologies). Cells were passaged and replicated once they were 80% confluent to increase cell volume. VSMCs used in the experiments were from passages 5 through 8. Each cell type used in this study was subjected to 5 different media conditions, with different antibodies, to assess the influence of cellular interactions. The control media used for all experiments was: DMEM supplemented with 10% FBS and 1% streptomycin/penicillin. The culture conditions were varied by mixing the control media with different antibodies at a 5-μg/ml concentration (33). The list of antibodies used along with their manufacturer details are summarized in Table **0**.**1**.

CMs were subjected to following media conditions:

control, control + 5 μg/ml IgG, control + 5 μg/ml anti-integrin β1, control + 5 μg/ml anti-connexin 43 and control + 5 μg/ml of both anti-connexin 43 and anti-integrin β1.

VSMCs were treated with following media conditions:

control, control + 5 μg/ml IgG, control + 5 μg/ml anti-integrin β1, control + 5 μg/ml monoclonal anti-N-Cadherin and control + 5 μg/ml of both anti-N-Cadherin and anti-integrin β1.

In order to explain the importance of culturing cells in 3D, we first performed experiments on CM cultured in monolayer and compared the results it to a freshly dissected neonatal rat heart. Significant differences were measured in apparent elastic modulus of cells in monolayer compared to that of heart tissue. Studies also involved culturing cardiomyocytes microtissues with fibroblast inhibitor cytosine arabinoside (AraC) and measuring cell mechanics.

Table 0.1: Summary of antibodies (Ab) used

Antibodies (Ab)	***Manufacturer***	***Type***	***Ab for CMs***	***Ab for VSMCs***
Anti-integrin β1	Sigma Aldrich	Polyclonal Rabbit IgG	✓	✓
Anti-connexin 43	Sigma Aldrich	Polyclonal Rabbit IgG	✓	x
Anti-N-cadherin	Sigma Aldrich	Monoclonal Rat	x	✓
IgG	Sigma Aldrich	Rat IgG	✓	✓

Preparing cellular microtissues

CMs and SMCs microtissues (spheroids) for created using hanging drop technique (figure 1). The cell density of isolated CMs and passaged VSMCs was obtained using Scepter^{TM}2.0 cell counter (EMP Millipore). The suspension was then diluted with appropriate media conditions so as to have 5000 cells per 20-µl cell suspension droplets. For each media type, approximately 50 drops were carefully plated in two hydrophobic lids of 10 cm diameter tissue culture dishes. A water bath (8 ml PBS + 2 ml of control media) was created in the petri dish to avoid vaporization of cellular droplets. Cells were allowed to aggregate by gravity, by storing the petri dishes under standard cell culture conditions (37°C and 5% CO_2) immediately after plating. The suspended state of the drops provided the environment for spheroid formation to occur.

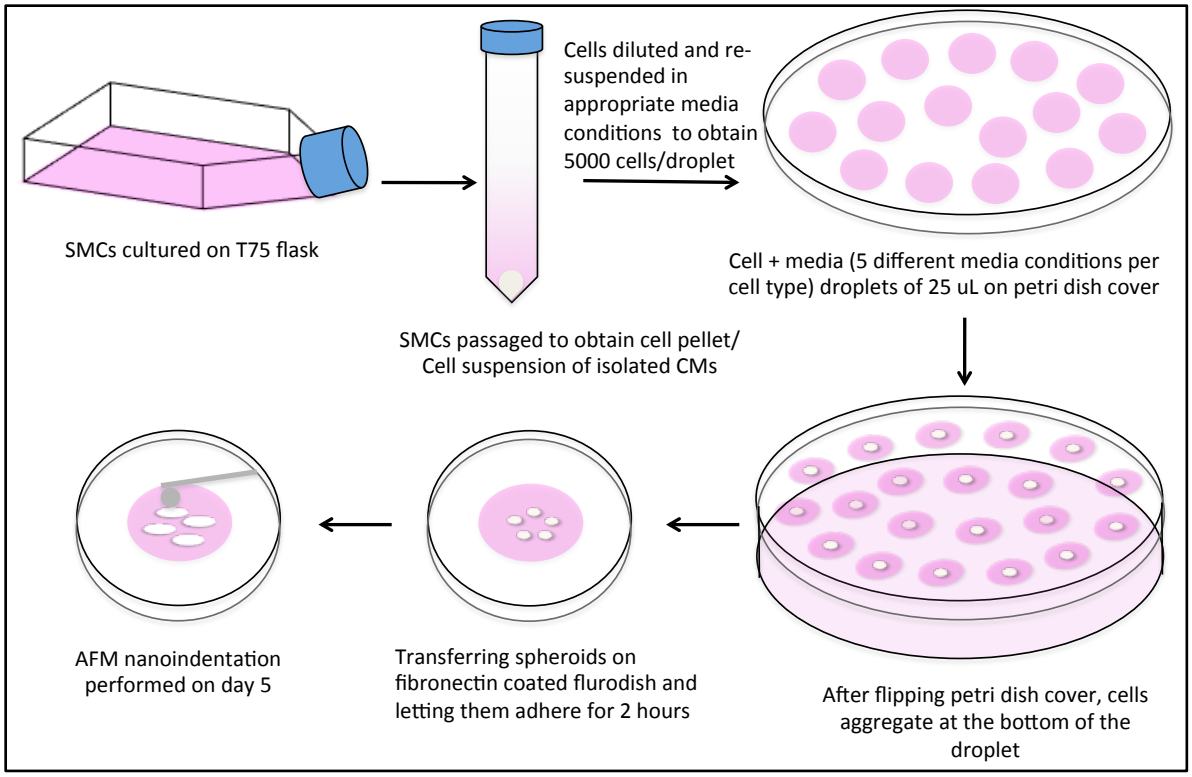

Figure 0.1: Schematic of the protocol followed to form cellular spheroids

Spheroid formation analysis

To assess spheroid formation, images were taken with a digital camera mounted on an upright optical microscope through the lid of the dish after 5, 7 and 10 days. From these images, the projected area of the spheroids was measured with image processing software ImageJ. All images were converted to simplified threshold images under the same converting conditions and the edges of the spheroids were then detected using a selection too. Feret's diameters of the detected spheroid edges were measured initially as pixels, and converted to micrometers by comparing to a reference length (18). For each media condition, at least 20 spheroids were imaged throughout all time points. Area of microtissues under each condition were calculated.

Atomic Force Microscopy (AFM) measurements

In order to transfer spheroids for AFM analysis, pipette tips were cut at the middle and used to suction individual drops to avoid disturbing the integrity of the spheroids. Five spheroids for each media condition were transferred to the middle of a poly-L-lysine (Sigma-Aldreich) coated Fluorodish®(world precision instruments). Fluorodishes were left in the incubator for 2h at 37°C, 5% CO_2 for the spheroids to attach to the bottom.

Once the spheroids were attached to the flurodishes, AFM measurements were performed. All AFM experiments were carried out using Asylum Research MFP-3D AFM (Asylum Research, Santa Barbara, CA, USA) in contact mode under fluid conditions. 5 μm diameter borosilicate prove with silicon nitride triangular cantilever (450 μm length, 50 μm width) (CP-PNP-BSG, NanoandMore, USA) was used to mechanically probe each spheroid. Before each experiment, the deflection sensitivity (nm/V) was measured by indenting into a clean glass Fluorodish® in water. The tip was also calibrated prior to each experiment using thermal calibration in order to use the most accurate spring constant measures for calculations. The spring constant of the tip used ranged from 0.221 - 0.457 N/m.

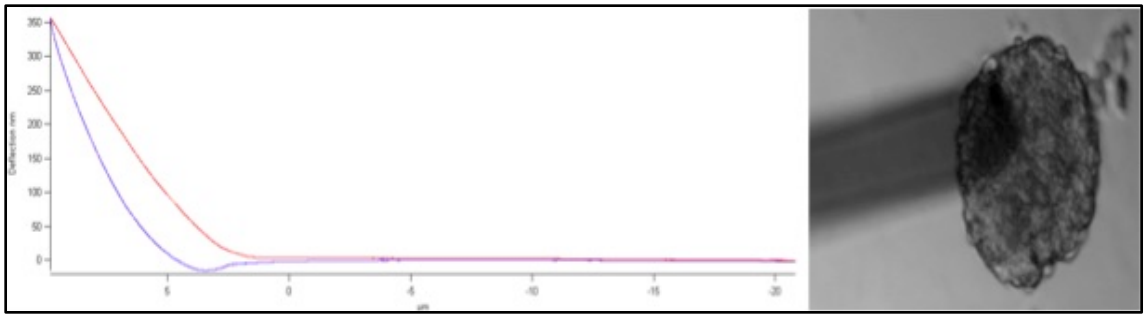

Figure 0.2: Raw data collected from AFM. (L) Raw data: typical deflection of the cantilever vs. piezo movement graph obtained from AFM indentation. (R) AFM cantilever aligned on a cardiomyocyte microtissue before indentation.

For each condition, at least 6 indentations in 3 randomly chosen locations for 3 spheroids were made at 2-4 μm/s at a scan rate of 0.1-0.2 Hz. The force-distance curves were exported from the AFM Software and converted with custom written MATLAB script (MathWorks, Natick, MA, USA) to normalize the contact point. Contact point was defined as the point where the slope of the curve changed, with a slope sensitivity that varied from 0.005 to 0.01, depending on the level of noise. The stiffness (apparent elastic modulus) was then calculated using the spherical Hertz contact mode, according to the following equation:

$$F = \frac{4}{3}\frac{E}{(1-\upsilon^2)}\sqrt{R\delta^3}$$

Where F is the measured force (N), E is the apparent elastic modulus calculated (Pa), R is the probe radius (m), υ is the Poisson's ratio (0.5) (5) and δ is the indentation depth (m).

One-way ANOVA with Tukey Test for means comparisons with $p<0.05$ significance was used for statistical analysis of AFM results on the software Origin 8.5.

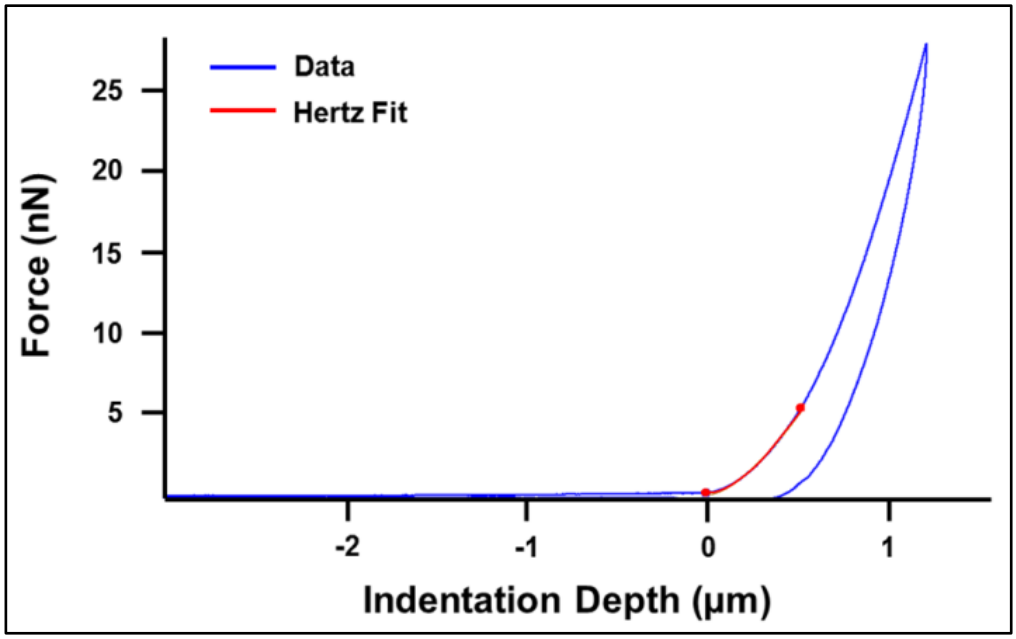

Figure 0.3: Sample force curve with Hertz model fit to the first 500nm of indentation

Scanning electron micrograph (SEM)

SEM was performed on the CM microtissues to study the effects of AraC on the phenotype of the spheroids. Following protocol was followed to prepare spheroids for SEM:

Primary Fixation: Immerse sample in 2.5% glutaraldehyde in 0.1M Cacodylate buffer, pH 7.4 for 2 hours at room temperature or at 4° C (in refrigerator) overnight.

Primary Wash: 3 washes (each 5 minute duration) in 0.1 M cacodylate buffer pH 7.4

Secondary Fixation: Immerse sample in 1% osmium tetroxide (aqueous) pH 7.4 for 1 hour at room temperature and in a light tight container.

Secondary Wash: 3 washes (each 5 minute duration) in 0.1 M cacodylate buffer pH 7.4

Dehydration: 1 x 10 min. in 25% ethanol1 x 10 min. in 50% ethanol1 x 10 min. in 70% ethanol1 x 10 min. in 85% ethanol1 x 10 min. in 95% ethanol2 x 10 min. in 100% ethanol1 x 10 min. in 100% ethanol (EM grade)

Critical Point Dry: This automated process takes approximately 40 minutes to complete.

Mounting: Mount the sample, which is now completely dried, onto metal stub with double-sided carbon tape.

Immunostaining

Fixation

The spheroid staining protocol from Weiswald *et al.* (34) was followed with some modifications. Approximately 5 spheroids for each condition on day 5 were fixed and impermeabilized with a solution of PBS with 4% paraformaldehyde (PFA) and 1% Triton X-100 for 3h at 4°C. Afterwards, the samples were washed 3 times in PBS, lasting 10 min each. Then, dehydration and rehydration in methanol of different concentrations at 4°C in PBS followed: 25% (15 min), 50% (15 min), 75% (15 min), 95% (15 min), 100% (2h), 95% (15 min), 75% (15 min), 50% (15 min), 25% (15 min). Next, the samples were washed in PBS (3 x 10 min). At this point, samples could be stored up to one month.

Staining

The samples were blocked overnight at 4°C in a solution of PBST – PBS + 0.1% Triton X-100 containing 3% Bovine Serum Albumin (BSA). Then, they were washed with PBST 2 times for 15 min. Since the samples already had primary antibodies in them,

they were incubated with secondary antibodies for 24h at 4°C. Washing step with PBS lasting 10 min followed this. Actin was stained with Phalloidin 488 for an hour followed by DAPI staining for nuclei for 30 min. Samples were than washed with PBS (thrice, 10 min each) and stored at 4°C in PBS until ready to image.

Table 0.2: Summary of the specific stains used to confirm blocking of cellular interactions

CMs Microtissues		**VSMCs Microtissues**	
Media conditions (1°Ab used)	Staining and (2°Ab used)	Media conditions (1°Ab used)	Staining and (2°Ab used)
No antibody control	Phalloidin 488, DAPI	No antibody control	Phalloidin 488, DAPI
Anti-integrin β1 in rabbit	TRITCI anti-rabbit, Phalloidin 488, DAPI	Anti-integrin β1 in rabbit	TRITCI anti- rabbit, Phalloidin 488, DAPI
Anti-connexin 43 in rabbit	Cy 7 anti-rabbit, Phalloidin 488, DAPI	Anti-N-cadherin in mouse	Alexa fluor anti-mouse, Phalloidin 488, DAPI
Anti-integrin β1 in rabbit + Anti-connexin 43	TRITCI anti-rabbit, Cy 7 anti-rabbit, Phalloidin 488, DAPI	Anti-integrin β1 in rabbit + Anti-N-cadherin	TRITCI anti- rabbit, Alexa fluor anti-mouse Phalloidin 488, DAPI

1.16 Results

CM blocking studies on adherent cells

In order to explain the importance of culturing cells in 3D, we first performed experiments on CM cultured in monolayer and compared the results it to a freshly dissected neonatal rat heart. Significant differences were measured in apparent elastic modulus of cells in monolayer compared to that of heart tissue.

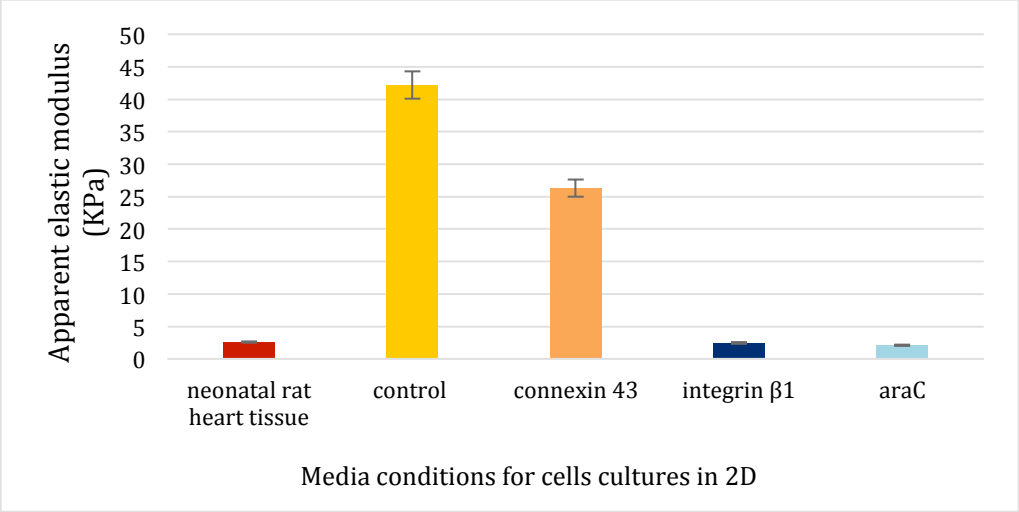

Figure 0.4: Apparent elastic modulus of CM cultured on traditional 2D surface at day 5 in culture compared to that of three day old neonatal rat heart Data presented percent error.

CM Microtissues

We are successfully able to form cardiomyocyte spheroids under antibody blocking conditions (Figure **0**.**5**). Results suggest that there is no significant difference in the volume of control and experimental conditions of spheroids over days 4 through 7 in culture. Differences in the area (Figure **0**.**6**) of spheroids at day 3 and day 10 in culture are indicative of the rate of spheroid formation as well as disintegration under various conditions.

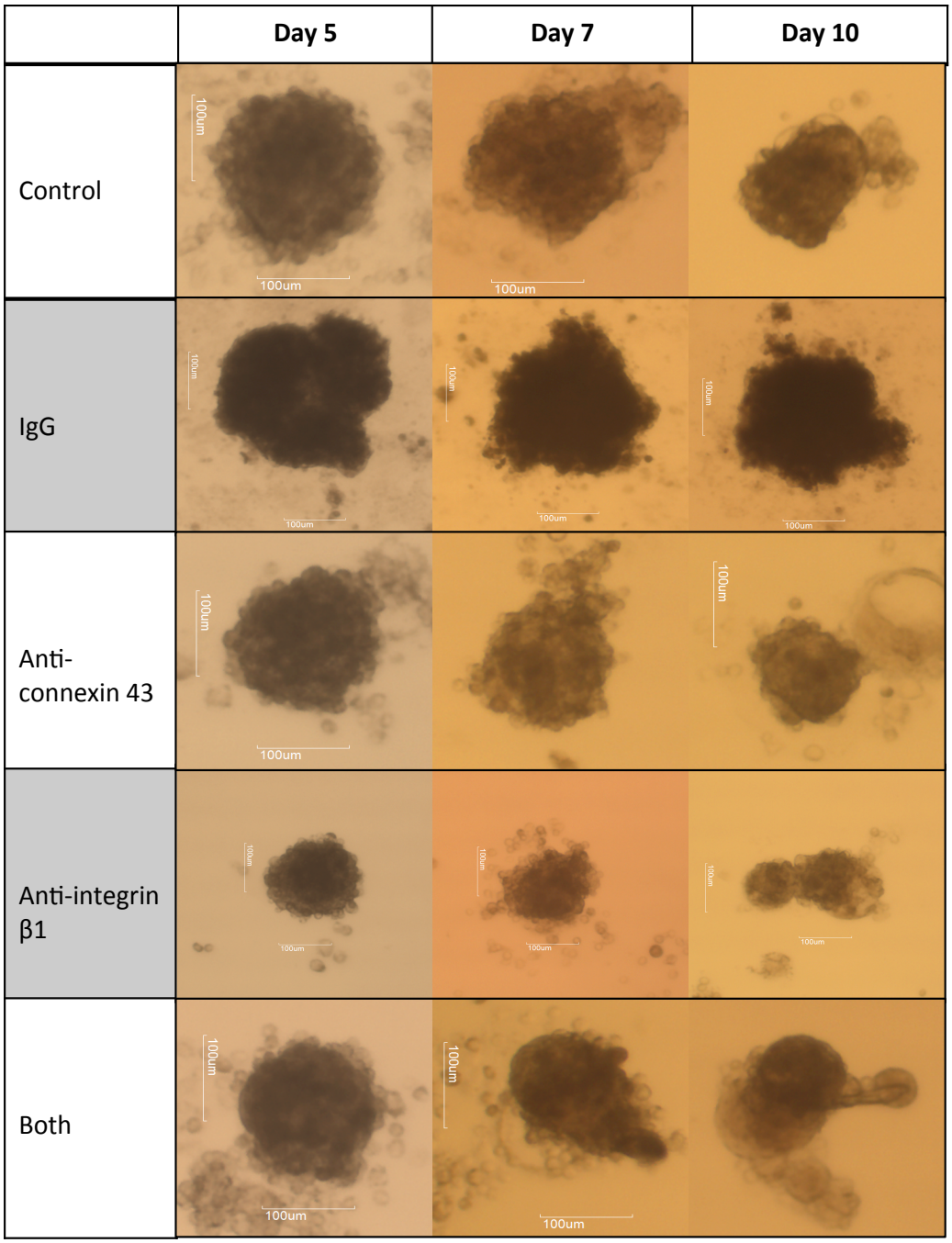

Figure 0.5: Pictures of cardiomyocyte microtissues in culture under different media conditions using hanging drop technique over a period of 10 days. Scale bar ' ——— ' = 100 µm

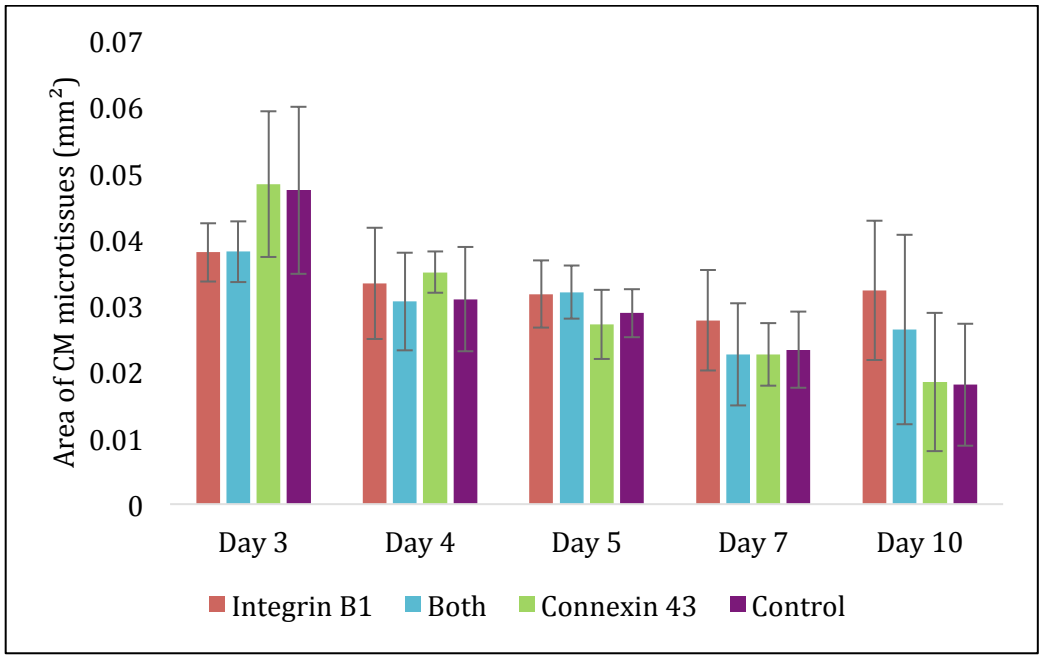

Figure 0.6: Analysis of area of cardiac microtissues under different media conditions over 10 days in hanging drop culture. Data presented as mean ± SD

The mean apparent elastic moduli of day 5 cardiomyocyte microtissues with different media conditions are shown in Figure **0**.**7**. The cells with no antibodies control and IgG control had average elastic moduli of 4.34 kPa and 5.26 kPa respectively. The cells under experimental (with antibodies) conditions had elastic moduli ranging from 3.87 kPa to 4.11 kPa. The drop is elastic moduli in experimental studies compared to control were considered statistically significant ($p<0.05$) in most cases. Both, anti-integrin β1 and anti-connexin 43 groups were significantly less stiff compared to control groups. All the antibody groups were significantly different from each other. The microtissues with antibodies were significantly less stiff compared to IgG control. The samples with connexin 43 antibodies were least stiff. There was no significant difference was observed on replicate indentations at same cellular location on each microtissue.

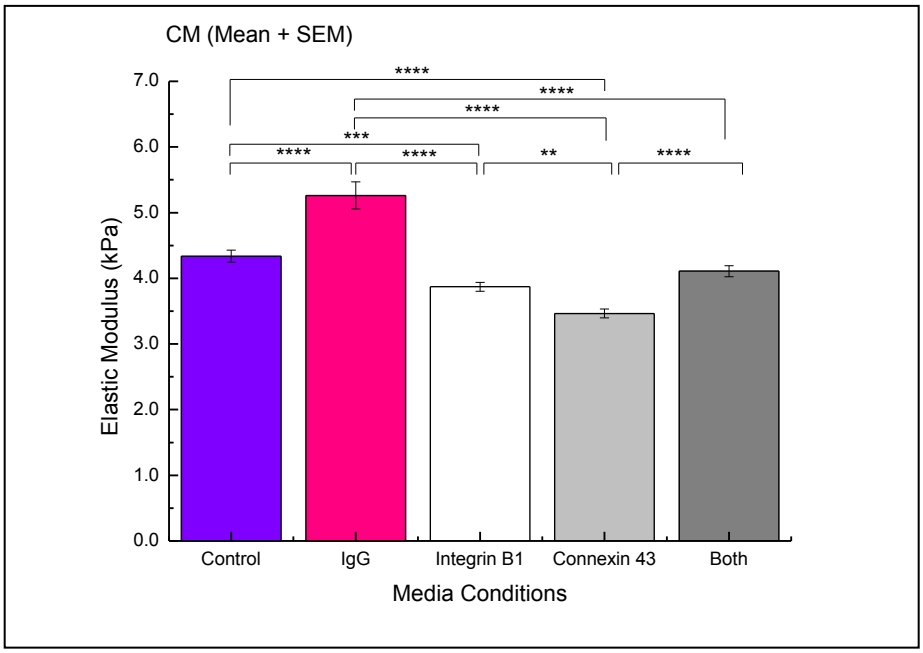

Figure 0.7: The apparent elastic moduli of cardiomyocyte microtissues under different media conditions at day 5 in culture (*p<0.05, **p<0.01, ***p<0.001, ****p<0.0001).

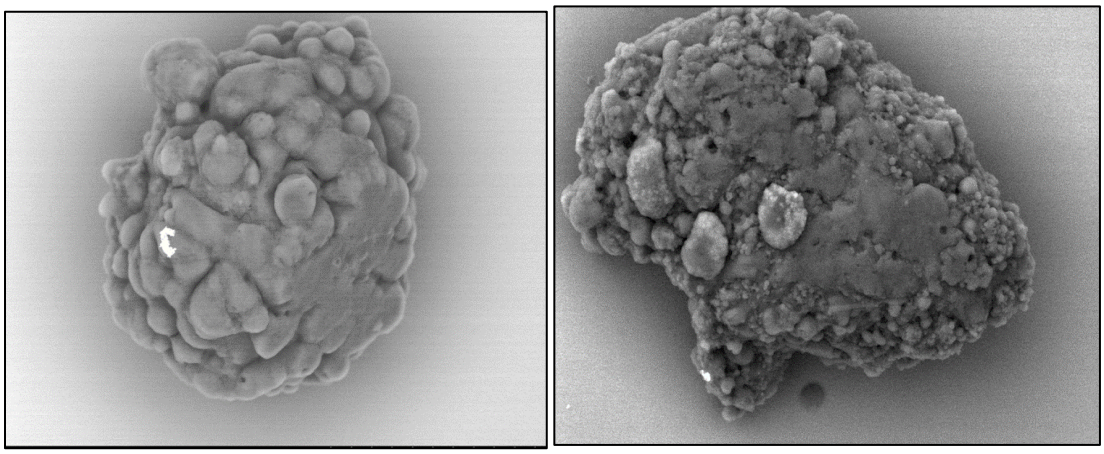

Figure 0.8: Scanning electron micrographs (SEM) displaying day 4 microtissues of cardiomyocytes.(L) Microtissues treated with control media. Cells produce extensive ECM within which the cells are held and barely distinguishable. (R) Microtissues treated with AraC media. The surface appears rough indicating AraC affects cellular environment.

VSMC Microtissues

We are successfully able to form cardiomyocyte spheroids under antibody blocking conditions Figure **0.10**. Analysis of the area (Figure **0.9**) of the spheroids suggests that spheroids blocking cell-cell interactions individually and in combination affects the rate and compactness of spheroid formation.

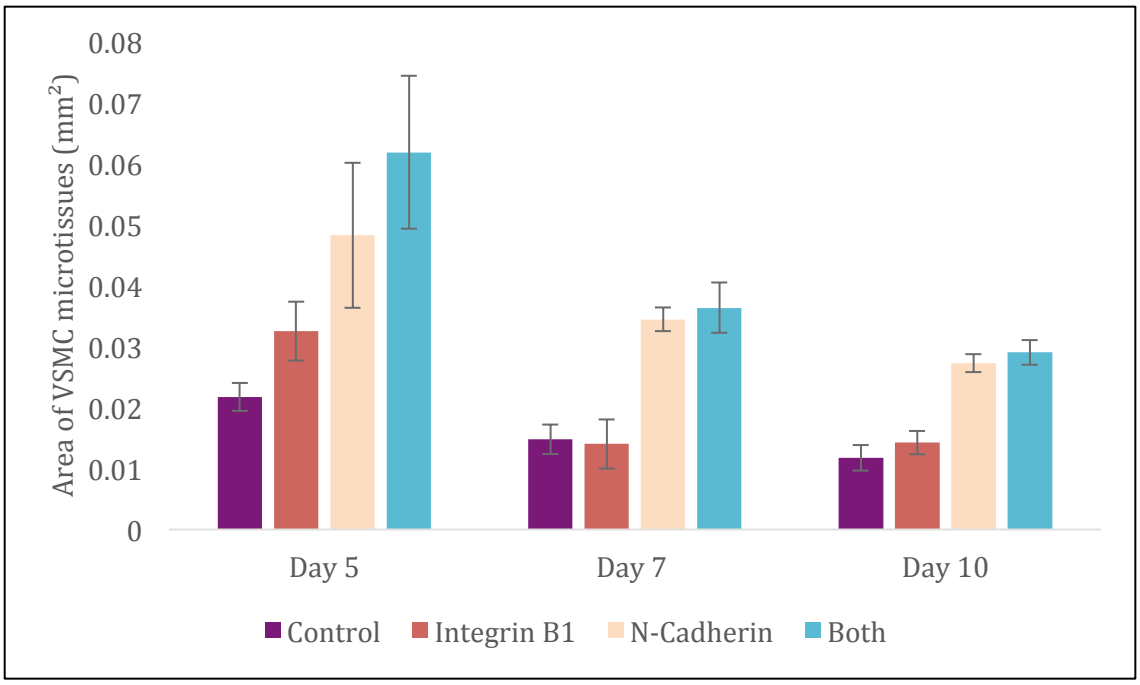

Figure 0.9: Analysis of area of vascular smooth muscle cell microtissues under different media conditions over 10 days in hanging drop culture. Data presented as mean ± SD.

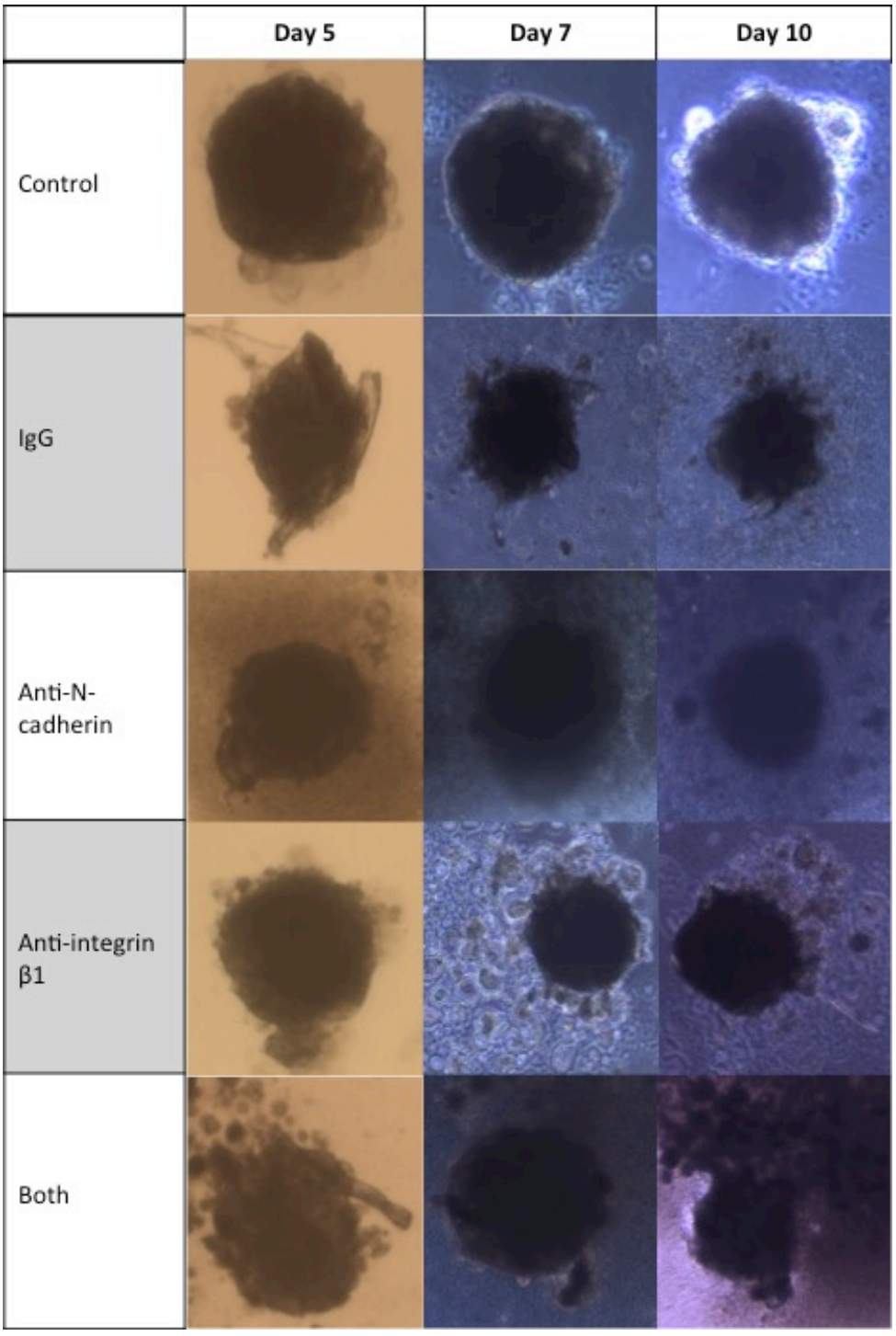

Figure 0.10: Pictures of vascular smooth muscle cell microtissues cultured in different media conditions using hanging drop technique over a period of 10 days.

Scale bar ‘ ——— ‘ = 100µm.

The mean apparent elastic moduli of day 5 cardiomyocyte microtissues with different media conditions are shown in figure 9. The cells with no antibodies control and IgG control had average elastic moduli of 3.68 kPa and 3.38 kPa respectively. The cells under experimental (with antibodies) conditions had elastic moduli ranging from 2.86 kPa to 4.12 kPa. No significant drop in modulus was observed in experimental conditions compared to control conditions, except for N-cadherin sample which were significantly ($p<0.05$) stiffer compared to IgG control. All the antibody groups were significantly different from each other. The samples with both antibodies were least stiff. There was no significant difference was observed on replicate indentations at same cellular location on each microtissue.

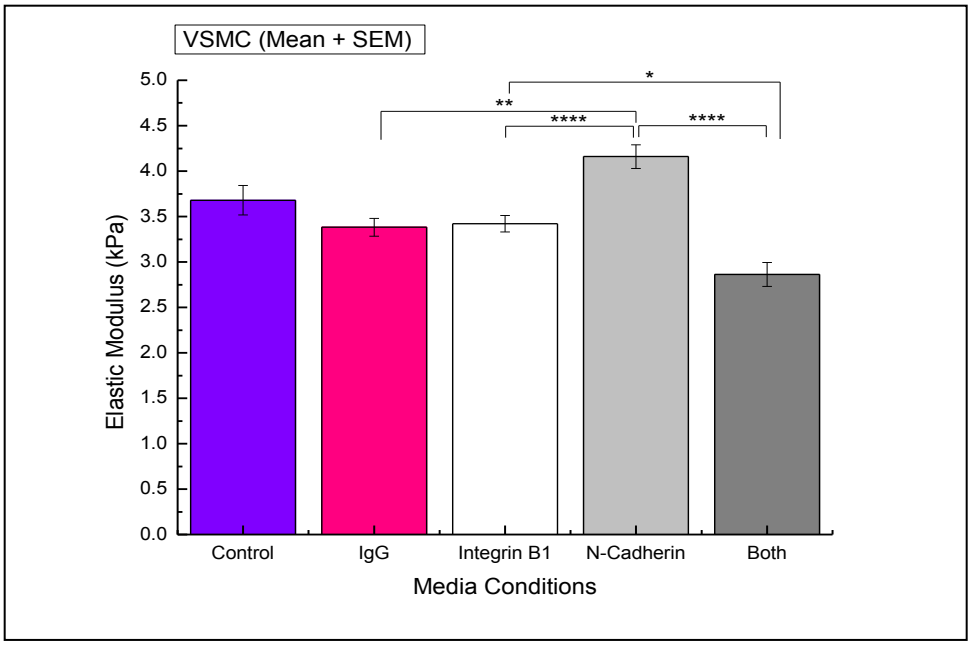

Figure 0.11: The apparent elastic moduli of vascular smooth muscle cell microtissues under different media conditions at day 5 in culture (*$p<0.05$, **$p<0.01$, ***$p<0.001$, ****$p<0.0001$).

1.17 Discussion and conclusion

Tissue elasticity is a highly regulated determinant of normal tissue development and function (35). Several studies have shown progressive stiffening on the extracellular matrix (ECM) in diseases including but not limited to cancer, cirrhosis, pulmonary fibrosis, and vascular diseases (36-39). Cell-cell and cell-ECM interactions are dynamic sites of chemical and mechanical stimuli that govern multiple phenomena, including cell sorting, wound healing, and tissue reorganization (40, 41).

Here, we studied the effects of blocking specific cellular interaction individually and in combination on the mechanics of cardiomyocyte and vascular smooth muscle cell microtissues. Previous studies involving inhibition of cell-cell and cell-matrix interactions have focused on studying the effects of blocking on cell proliferation, migration, differentiation, adhesion, disease progression, and apoptosis (42-48). However, this is the first study that investigates the role of integrin β1, connexins 43, and N-cadherin mediated cellular interactions on mechanical properties of cardiovascular cells in scaffold free 3D culture system.

Our results from cell-cell and cell-matrix interactions individually and in combination indicate significant drop in cellular stiffness in cardiac microtissues. However, the results from VSMC microtissues do not follow the same trend. VSMC studies show and increase in cellular stiffness by blocking cell-cell interactions. Interestingly, our results from blocking studies in microtissue follow similar trends to the blocking studies on 2D, adherent culture previously done in our lab. Blocking studies in 2D have resulted in elastic moduli ranging from 2.3 kPa to 5.3 kPa under experimental

conditions, a significant drop compared to no antibody (8.6 kPa) and IgG (10.6 kPa) control conditions. Increase in stiffness of VSMCs spheroids on blocking N-cadherin interactions have been consistent with previous studies done in our lab in on VSMCs cultured on polyacrylamide gels, Charras et.al. (33) observed similar results by blocking E-cadherin interactions on epithelial cells on collagen gels.

Through this study, we were for the first time able to make cellular microtissues of CMs and SMCs with the use of antibodies that block specific cellular interactions. This allowed us to replicate in vivo like cellular microenvironment as microtissues are shown to be better representative models of tissue like environment compared to adherent culture system. Our results indicate that cell stiffness changes under antibody blocking conditions in both cardiomyocyte as well as smooth muscle cells. Blocking cell-matrix interactions of integrin β1 results in decrease in stiffness of cells. However, blocking cell-cell interactions of connexin 43 in CMs results in less stiff less, whereas N-cadherin blocking in VSMCs results in significantly stiffer cells. Elastic modulus values suggest that integrin β1, connexins 43, and N-cadherin play an important role in determining cellular mechanical properties.

The influence of connexin 43 and N-cadherin mediated cell-cell interactions and integrin β1 mediated cell-matrix interactions on elastic modulus of cellular microtissues were assessed for the first time in this study. Blocking these interactions individually and in combination resulted in reduced cellular elastic modulus in both CMs and SMCs (except anti N-cadherin media condition).

These results provide researchers with better understanding of the role of cellular adhesions in regulating mechanical properties at tissue scale.

1.18 References

1. Thomas G, Burnham NA, Camesano TA, Wen Q. Measuring the mechanical properties of living cells using atomic force microscopy. JoVE (Journal of Visualized Experiments). 2013(76):e50497-.

2. Discher DE, Janmey P, Wang YL. Tissue cells feel and respond to the stiffness of their substrate. Science. 2005 Nov 18;310(5751):1139-43.

3. Cross SE, Jin Y, Lu Q, Rao J, Gimzewski JK. Green tea extract selectively targets nanomechanics of live metastatic cancer cells. Nanotechnology. 2011;22(21):215101.

4. Rotsch C, Radmacher M. Drug-induced changes of cytoskeletal structure and mechanics in fibroblasts: an atomic force microscopy study. Biophys J. 2000;78(1):520-35.

5. Mahaffy R, Park S, Gerde E, Käs J, Shih C. Quantitative analysis of the viscoelastic properties of thin regions of fibroblasts using atomic force microscopy. Biophys J. 2004;86(3):1777-93.

6. Chen CS, Tan J, Tien J. Mechanotransduction at cell-matrix and cell-cell contacts. Annu Rev Biomed Eng. 2004;6:275-302.

7. Schwartz MA, DeSimone DW. Cell adhesion receptors in mechanotransduction. Curr Opin Cell Biol. 2008;20(5):551-6.

8. Geiger B, Spatz JP, Bershadsky AD. Environmental sensing through focal adhesions. Nature reviews Molecular cell biology. 2009;10(1):21-33.

9. le Duc Q, Shi Q, Blonk I, Sonnenberg A, Wang N, Leckband D, et al. Vinculin potentiates E-cadherin mechanosensing and is recruited to actin-anchored sites within adherens junctions in a myosin II-dependent manner. J Cell Biol. 2010 Jun 28;189(7):1107-15.

10. Feinberg AW, Feigel A, Shevkoplyas SS, Sheehy S, Whitesides GM, Parker KK. Muscular thin films for building actuators and powering devices. Science. 2007 Sep 7;317(5843):1366-70.

11. Au HTH, Cheng I, Chowdhury MF, Radisic M. Interactive effects of surface topography and pulsatile electrical field stimulation on orientation and elongation of fibroblasts and cardiomyocytes. Biomaterials. 2007;28(29):4277-93.

12. Au HTH, Cui B, Chu ZE, Veres T, Radisic M. Cell culture chips for simultaneous application of topographical and electrical cues enhance phenotype of cardiomyocytes. Lab on a chip. 2009;9(4):564-75.

13. Zhang P, Su J, Mende U. Cross talk between cardiac myocytes and fibroblasts: from multiscale investigative approaches to mechanisms and functional consequences. Am J Physiol Heart Circ Physiol. 2012 Dec 15;303(12):H1385-96.

14. Samarel AM. Costameres, focal adhesions, and cardiomyocyte mechanotransduction. Am J Physiol Heart Circ Physiol. 2005 Dec;289(6):H2291-301.

15. Souders CA, Bowers SL, Baudino TA. Cardiac fibroblast: the renaissance cell. Circ Res. 2009 Dec 4;105(12):1164-76.

16. Camelliti P, Borg TK, Kohl P. Structural and functional characterisation of cardiac fibroblasts. Cardiovasc Res. 2005 Jan 1;65(1):40-51.

17. Luo Y, Radice GL. Cadherin-mediated adhesion is essential for myofibril continuity across the plasma membrane but not for assembly of the contractile apparatus. J Cell Sci. 2003 Apr 15;116(Pt 8):1471-9.

18. Han C, Takayama S, Park J. Formation and manipulation of cell spheroids using a density adjusted PEG/DEX aqueous two phase system. Scientific reports. 2015;5.

19. Abbott A. Cell culture: biology's new dimension. Nature. 2003;424(6951):870-2.

20. Yamada KM, Cukierman E. Modeling tissue morphogenesis and cancer in 3D. Cell. 2007;130(4):601-10.

21. Baker M. Tissue models: a living system on a chip. Nature. 2011;471(7340):661-5.

22. Griffith LG, Swartz MA. Capturing complex 3D tissue physiology in vitro. Nature reviews Molecular cell biology. 2006;7(3):211-24.

23. Pampaloni F, Reynaud EG, Stelzer EH. The third dimension bridges the gap between cell culture and live tissue. Nature reviews Molecular cell biology. 2007;8(10):839-45.

24. Huh D, Hamilton GA, Ingber DE. From 3D cell culture to organs-on-chips. Trends Cell Biol. 2011;21(12):745-54.

25. Sutherland RM. Cell and environment interactions in tumor microregions: the multicell spheroid model. Science. 1988 Apr 8;240(4849):177-84.

26. Friedrich J, Seidel C, Ebner R, Kunz-Schughart LA. Spheroid-based drug screen: considerations and practical approach. Nature protocols. 2009;4(3):309-24.

27. Sutherland R, Carlsson J, Durand R, Yuhas J. Spheroids in cancer research. Cancer Res. 1981;41(7):2980-4.

28. Mehta G, Hsiao AY, Ingram M, Luker GD, Takayama S. Opportunities and challenges for use of tumor spheroids as models to test drug delivery and efficacy. J Controlled Release. 2012;164(2):192-204.

29. Hsiao AY, Torisawa Y, Tung Y, Sud S, Taichman RS, Pienta KJ, et al. Microfluidic system for formation of PC-3 prostate cancer co-culture spheroids. Biomaterials. 2009;30(16):3020-7.

30. Tekin H, Anaya M, Brigham MD, Nauman C, Langer R, Khademhosseini A. Stimuli-responsive microwells for formation and retrieval of cell aggregates. Lab on a chip. 2010;10(18):2411-8.

31. Kim JA, Choi J, Kim M, Rhee WJ, Son B, Jung H, et al. High-throughput generation of spheroids using magnetic nanoparticles for three-dimensional cell culture. Biomaterials. 2013;34(34):8555-63.

32. Liu H, Qin W, Shao Y, Ma Z, Ye T, Borg T, et al. Myofibrillogenesis in live neonatal cardiomyocytes observed with hybrid two-photon excitation fluorescence-second harmonic generation microscopy. J Biomed Opt. 2011;16(12):126012-1260124.

33. Harris AR, Daeden A, Charras GT. Formation of adherens junctions leads to the emergence of a tissue-level tension in epithelial monolayers. J Cell Sci. 2014 Jun 1;127(Pt 11):2507-17.

34. Weiswald L, Guinebretière J, Richon S, Bellet D, Saubaméa B, Dangles-Marie V. In situ protein expression in tumour spheres: development of an immunostaining protocol for confocal microscopy. BMC Cancer. 2010;10(1):1.

35. Sazonova OV, Lee KL, Isenberg BC, Rich CB, Nugent MA, Wong JY. Cell-cell interactions mediate the response of vascular smooth muscle cells to substrate stiffness. Biophys J. 2011;101(3):622-30.

36. Matsumoto T, Abe H, Ohashi T, Kato Y, Sato M. Local elastic modulus of atherosclerotic lesions of rabbit thoracic aortas measured by pipette aspiration method. Physiol Meas. 2002;23(4):635.

37. Suki B, Bates JH. Extracellular matrix mechanics in lung parenchymal diseases. Respiratory physiology & neurobiology. 2008;163(1):33-43.

38. Zhao G, Cui J, Qin Q, Zhang J, Liu L, Deng S, et al. Mechanical stiffness of liver tissues in relation to integrin β1 expression may influence the development of hepatic cirrhosis and hepatocellular carcinoma. J Surg Oncol. 2010;102(5):482-9.

39. Vernhet H, Demaria R, Perez-Martin A, Juan JM, Oliva-Lauraire MC, Marty-Double C, et al. Wall mechanics of the stented rabbit aorta: long-term study and correlation with histological findings. J Endovasc Ther. 2003 Jun;10(3):577-84.

40. Leckband D, Prakasam A. Mechanism and dynamics of cadherin adhesion. Annu Rev Biomed Eng. 2006;8:259-87.

41. Yap AS, Brieher WM, Gumbiner BM. Molecular and functional analysis of cadherin-based adherens junctions. Annu Rev Cell Dev Biol. 1997;13(1):119-46.

42. Koutsouki E, Beeching CA, Slater SC, Blaschuk OW, Sala-Newby GB, George SJ. N-cadherin-dependent cell-cell contacts promote human saphenous vein smooth muscle cell survival. Arterioscler Thromb Vasc Biol. 2005 May;25(5):982-8.

43. McNally AK, Anderson JM. β1 and β2 integrins mediate adhesion during macrophage fusion and multinucleated foreign body giant cell formation. The American journal of pathology. 2002;160(2):621-30.

44. Hermiston ML, Gordon JI. In vivo analysis of cadherin function in the mouse intestinal epithelium: essential roles in adhesion, maintenance of differentiation, and regulation of programmed cell death. J Cell Biol. 1995 Apr;129(2):489-506.

45. Steinberg MS, McNutt PM. Cadherins and their connections: adhesion junctions have broader functions. Curr Opin Cell Biol. 1999;11(5):554-60.

46. Li G, Satyamoorthy K, Herlyn M. N-cadherin-mediated intercellular interactions promote survival and migration of melanoma cells. Cancer Res. 2001 May 1;61(9):3819-25.

47. Cheng S, Shin CS, Towler DA, Civitelli R. A dominant negative cadherin inhibits osteoblast differentiation. Journal of Bone and Mineral Research. 2000;15(12):2362-70.

48. Siebers M, Walboomers X, van den Dolder J, Leeuwenburgh S, Wolke J, Jansen J. The behavior of osteoblast-like cells on various substrates with functional blocking of integrin-β1 and integrin-β3. J Mater Sci Mater Med. 2008;19(2):861-8.

CHAPTER FIVE

CHARACTERIZING RADIAL AND AXIAL FORCES ON ISOLATED ADULT CARDIOMYOCYTES SIMULTANEOUSLY

1.19 Introduction

Cells are exposed to and must respond to variety of mechanical loads in vivo (1-4). The response to mechanical stimuli is complex and depends on the magnitude (5) of the force applied as well as its rate (6). Mechanical properties of cells are responsible for many physiological processes and their alteration can lead to impaired biological functions and diseases (7, 8). Cardiac cells, in particular, are highly mechano-sensitive. Cardiomyocytes and fibroblasts change their phenotype in response to mechanical strain [REF] and these responses, in turn, modulate cardiac tissue The heart's mechanical properties and behaviour, which depends on its constituent cells and extracellular matrix, are quite complex and directly affect the organ's function. Both the active and passive mechanical properties of cardiomyocytes contribute to cardiac tissue mechanical properties. Active and passive mechanical behaviours of cells are thought to be related (7). However, experimental techniques are usually adapted to characterize only one of these properties in one dimension at a time. Cardiomyocytes, as they contract generate forces in both axial and radial directions simultaneously. While axial forces generated by beating isolated cardiomyocytes have been described in detail, corresponding radial mechanics remains poorly characterised. It is difficult to interrelate axial and radial mechanics experimentally, and to decouple active and passive force components with any single technique known to us. For example, micropipette aspiration (9), magnetic twisting

cytometry (10), optical stretchers (11) are used to determine the rheological behaviour, whereas actively generated traction forces are measured through the deformation of compliant gels (12) or 2D arrays of micropillars (13). Optical tweezers (14, 15) using micromemetic beads as probes are used to measure local subcellular mechanics. Depending on the size of the probe used, atomic force microscopy (AFM) (16, 17) can be used to investigate mechanics of cells from sub cellular to whole cell level. Carbon fibre (CF) technique has also been used extensively to study myocardial mechanics and mechano-electric coupling (18, 19). Parallel plate technique (20, 21) also allows for the measurement of cell mechanics on single cell as well as cellular aggregates, depending on the shape and dimension of the flexible plate used as force probe. But, there is no single technique that can measure mechanics on a single cell simultaneously in axial as well as radial directions in both active as well as passive conditions.

To this end, our aim is to monitor simultaneously passive and active forces, both axially and radially, in ventricular cardiomyocytes freshly isolated from adult mouse. We propose a novel design that combines AFM and CF techniques under one set up. AFM is a popular technique used to probe mechanical response of cells (5, 22, 23). It has been used to measure both elastic (8) and viscous (3, 6, 24-27) cellular responses. AFM was used to apply and measure radial mechanics on a single cell. CF is a technique complimentary to AFM. It allows attachment of single isolated cardiomyocytes to carbon fibers for mechanical manipulation and measurement. CF's are adhesive to cells and can be attached to its membrane keeping the cells intact as they are known not to damage cells (19). The CF technique allows for measurement of both active and passive

mechanical properties of cardiomyocytes in axial direction. This manuscript describes the novel combination of AFM and CF techniques to characterize active and passive mechanics (force and stiffness) of a single isolated cardiomyocyte both radially and axially simultaneously.

1.20 Materials and methods

To be able to apply stretch and characterize axial and radial forces, we combine a carbon fiber (CF) setup with a custom-designed atomic force microscope (AFM) system.

Mouse Ventricular cardiomyocyte isolation

All experiments were carried out in accordance with the UK Home Office guidance on the Operations of Animals Act of 1986.

Perfusion chamber

A custom designed 3D printed was used to optimize cell perfusion, temperature control and pacing. The perfusion chamber consisted of a glass coverslip coated with poly-HEMA (2-hydroxyethyl methacrylate; Sigma, UK) to prevent cell adhesion and minimize friction while stretching. Cells were paced at the frequency of 2 Hz with. The solution flow was maintained in the chamber using the solenoid pinch–valve system.

Carbon Fiber (CF) technique

CF is a technique used to apply axial stretch on cells and measure active and passive forces. A pair of compliant, computer controlled and piezo positioned CFs attached to opposite ends of cell (glue free) are used to dynamically control the mechanical environment of isolated intact cardiomyocytes. To prepare the fibers, thin glass capillaries were pulled using pipette puller (PP-830, Narishige, Tokyo, Japan) from glass tubes (inner diameter: 1.16mm; outer diameter: 2.0mm) and a pair of CF was mounted on the fine tip of the pulled capillary. The narrow end of the capillary (holding CF) was thermally bent by 20° to allow parallel alignment of the fibers with the bottom of the chamber Figure **0.3**. The length of the CF protruding out of the capillary was maintained at 1.20mm and fixed with a cyanoacrylate-adhesive. A force transducer system was used to calibrate the stiffness of the CFs. The wider end of the glass tube was fitted in the holder of a hydraulic manipulator (MW-300; Narishige, Tokyo, Japan) for controlled lowering of CF tips onto the cells. The hydraulic manipulator was mounted on top of a piezotranslator (P-623.1CL; Precision Instruments GmbH, Karlsruhe, Germany), fixed on sleighs of a railing system (IonOptix, Milton, MA, USA), which was driven by custom written LabView™ script to allow accurate application of mechanical preloads (18).

Atomic Force Microscopy (AFM)

A custom designed AFM based on the LS-AFM design from AFM Workshop™, Signal Hill, CA, USA was used to characterize radial cell mechanics. The setup was

modified to give a large area for frontal access to fit CF set up underneath. To achieve an open-access AFM design, the laser path, tip holder, and sample stage had to be redesigned (Figure **0**.**1**); the new system also does not interfere with the optical capture of the CF technique. For mechanical testing, cytoindentation experiments were performed using a 5 μm diameter borosilicate spherical tipped probe on a silicon nitride cantilever (450 μm length and 50 μm width) with a spring constant of ~0.25 N/m (CP-PNP-BSG, NanoandMore, UK).

AFM-CF Alignment on cardiomyocyte

Selected cells were positioned in the center of the field of view, and aligned parallel to the front edge of the microscope stage. CF's were then lowered onto the opposite ends of a cardiomyocyte and the tips were attached to the cell. Once CF's were attached, perfusion in the system was started to maintain the temperature of the solution in the chamber. Following which, AFM tip was lowered making sure that the tip was aligned to the center of the cell.

Criteria for selecting cells for measurements

Only the cells that fulfilled the following criteria were used for measurements: i) rod-shaped cardiomyocytes with clear striations and well defined membrane free of granulations, ii) resting sarcomere length (SL) of at least 1.7 μm, and iii) lack of contraction in absence of electrical field simulation.

Data recording and analysis

Before performing any force measurements on cells, the deflection sensitivity of AFM tip was calbriated by indenting on a clean glass slide in water. In addition, the spring constant of the tip was calibrated using a spectrum analyzer (oscilloscope) (Vertins Technology, VT DSO-2810R). Peak frequency and minimum and maximum frequencies (peak width) were recorded and spring constant was calculated using Sader method (28).

Isolated cardiomyocytes were placed in the chamber and all three probes (a pair of CFs and AFM tip) were aligned on a single cell. For each cell was indented twice before applying mechanical load (stretch) to get baseline (control) data. Following which, stretch of up to 50 μm (quantified by change in SL) was applied and passive forces in radial and axial directions were measured. Stretch on cell applied by piezotranslator movement, was compared to CF tip movement and the bending was used to identify passive force. Cells were paced and CF bending during contraction was recorded to identify active force generated axially. AFM indentation was performed simultaneously to quantify radial forces.

CF positions and SL were monitored by a contrast-based detection system from IonOptix to quantitatively access cell deformation. Distance between CF tips gives accurate representation of effective cell lengthening as the cells are subjected to defined axial stretch. Sarcomere shortening was measured in real time, using fast Fourier transformation.

The force distance curve were exported from AFM software and analyzed with a custom written MATLAB script. Raw data from AFM, deflection of photodetector (Volts) vs. Z-piezo distance (nm) was converted to force (nN) vs. tip-sample separation distance (nm). The deflection was converted from Volts to nm using the deflection sensitivity parameter calibrated for each experiment. The indentation force was (F) was calculated using Hooke's law ($F = k\delta$) where k and δ denote the cantilevers spring constant and measured deflection of the cantilever respectively. (29, 30) The indentation depth was calculated from the difference in the z-piezo movement and the deflection of the cantilever. (29-32) Force data was further analyzed and active and passive radial forces under mechanical load were well as no load was recorded. Hertz's linear elastic model for spherical indenter was used to analyze cell indentation data.

$$F = \frac{4E}{3(1-\nu^2)} R^2 \delta^{\frac{3}{2}}$$

where E is the elastic modulus (Young's modulus), ν is the Poisson's ratio (0.45), R is the radius of the indenter, F is the force measured, and δ is the indentation depth.

1.21 Results

Atomic Force Microscopy (AFM) and Carbon Fiber (CF): A novel combination

This is a first report of quantifying radial and axial mechanics (forces) simultaneously on a single isolated cardiomyocyte. We successfully developed a set up that can combine AFM and CF techniques. AFM was custom designed and modified to enable frontal access to fit CF set up (Figure **0**.**1**, Figure **0**.**2**, Figure **0**.**3**). This set up, for

the first time allows for multidimensional measurement of cell mechanics. It can also be combined with patch clamp set up, to measure cell mechanics with AFM while also performing patch clamp simultaneously to measure ion channel activity.

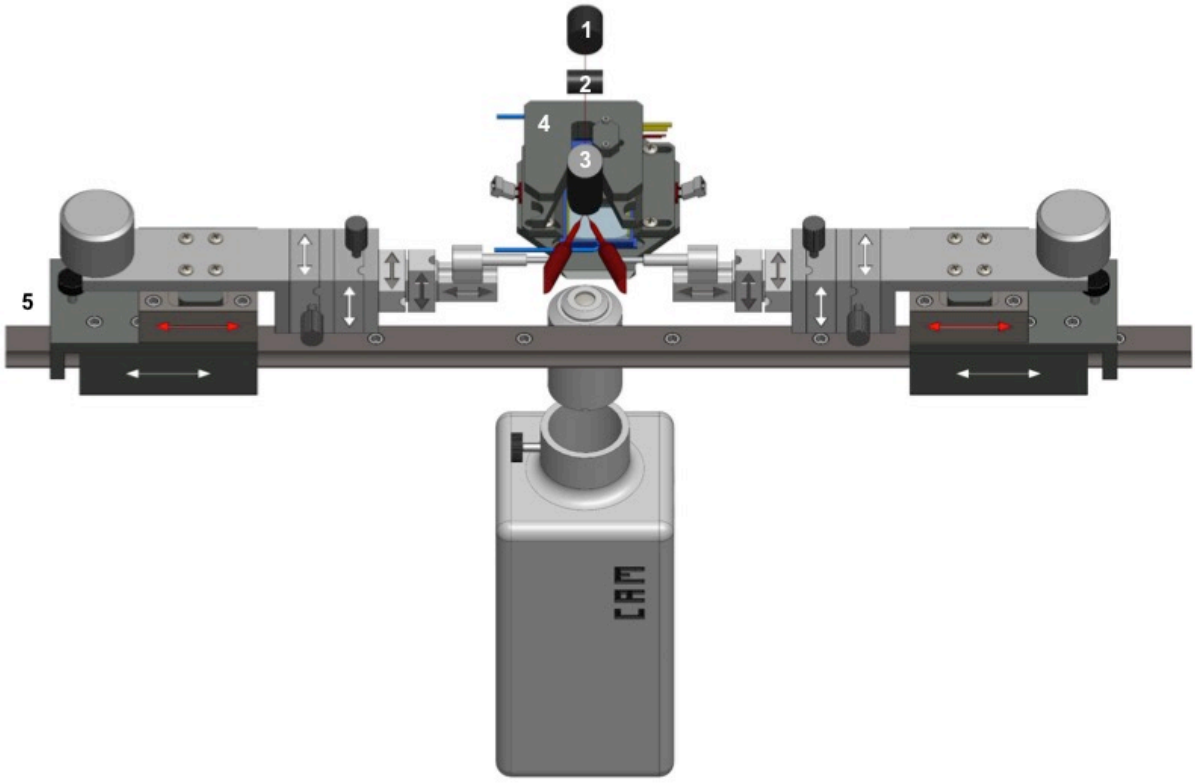

Figure 0.1: Schematic of general view of the set up combining CF and AFM techniques. AFM laser source (1), mirror (2) and detector (3) sit on the top of the tip holder (4), the latter standing above the perfusion chamber (blue). CF holders (red) are mounted on manual (white arrows) and mechanical (grey arrows) micromanipulators allowing fast and fine positioning of the fibres. This assembly is standing on a piezo micromanipulator (red arrows) achieving displacements with micrometres accuracy to control cell stretch. The entire CF set up is mounted on a railing system (5) ensuring CF movement parallel to a single plane and allowing fast macroscopic alignmen to fthe fibres with the perfusion chamber. Experiments are performed using an inverted microscope and the MyoCam-S™ camera from IonOptix optimised to record sarcomere length.

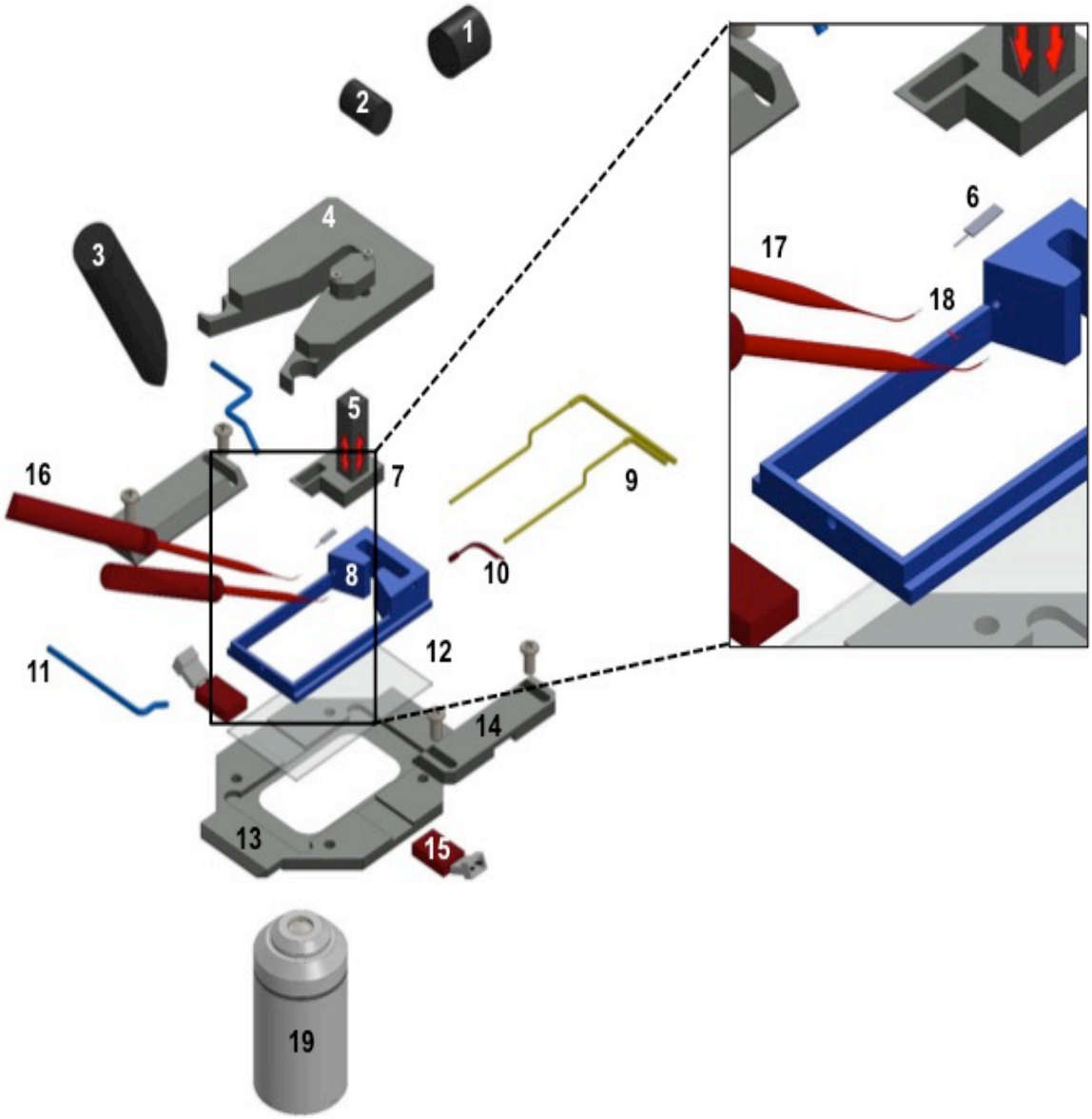

Figure 0.2: Exploded view of the AFM main components, perfusion chamber and CF. The laser source (1), the mirror (2) and the detector (3) sit above the light lever assembly composed of the holder (4), the z-piezo (5) and the tip (6) holder (7). Underneath, a 3D-printed perfusion chamber (8) was designed to optimise AFM and CF access. It welcomes two electrodes (9) for pacing, a temperature sensor (10) and tubing for in flow (11) and out flow (11') to perfuse cells and keep the temperature constant. The chamber and the glass coverslip (12) constituting the bottom are screwed to chamber's platform (13) by two holders (14). To help maintain the temperature the platform is heated (15) from both sides. CF holders (16) bring the bended glass capillaries (17) holding CF(18) in the field of view (19).

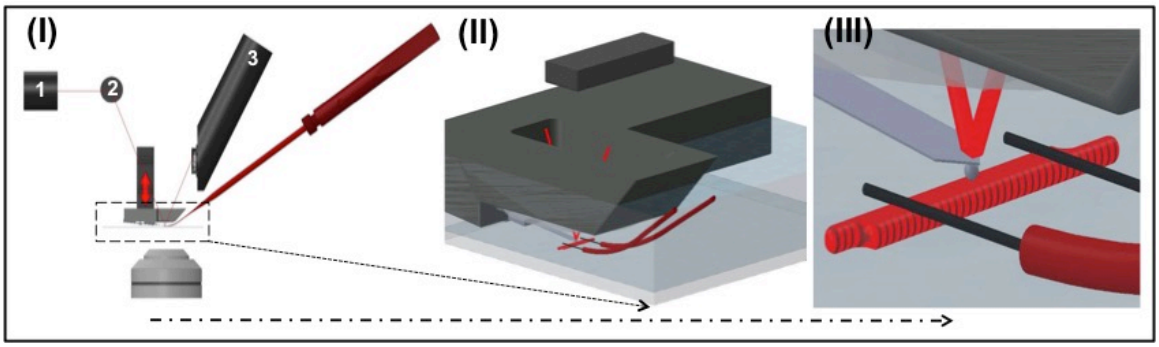

Figure 0.3: Side view of the AFM and CF setup. I) Detail of the laser path with a CF in working position. The laser is emitted at the back of the setup, is guided by a mirror to the tip of the cantilever, which reflects it to a detector (3). II) and III) show the AFM light lever and the two CF aligned with a single isolated cardiomyocyte.

CF movement and sarcomere length detection

Distance between CF tips represented effective cell-length involved in contraction/relaxation and being subjected to defined axial stretch. Cells were stretched up to a distance of 50 µm (motor displacement distance) in increments of 5, 10, 15, 20, 30, 40, and 50 µm with CFs. The amount of stretch applied was quantified (actual cell strain) by calculating the change in sarcomere length upon CF displacement. CF length was calculated to have increased by up to 10% as the piezotranslators were moved up to distance of 50 µm.

An increase in strain applied to the cell with CFs also resulted in an increase in the axial force measured. As the amount of stretch applied to cell increased from 0 to 50 µm, the axial force increased linearly from 0 to 0.4 µN.

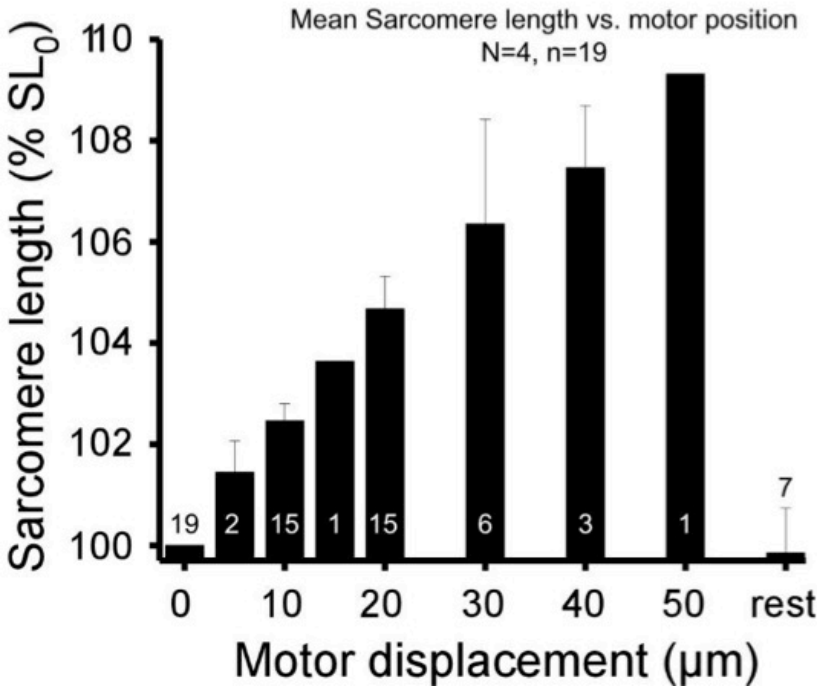

Figure 0.4: Sarcomere elongation in response to stretch (CF displacement). The % change in sarcomere length increased linearly with motor displacement. N = 4 mice, n = 19 cells

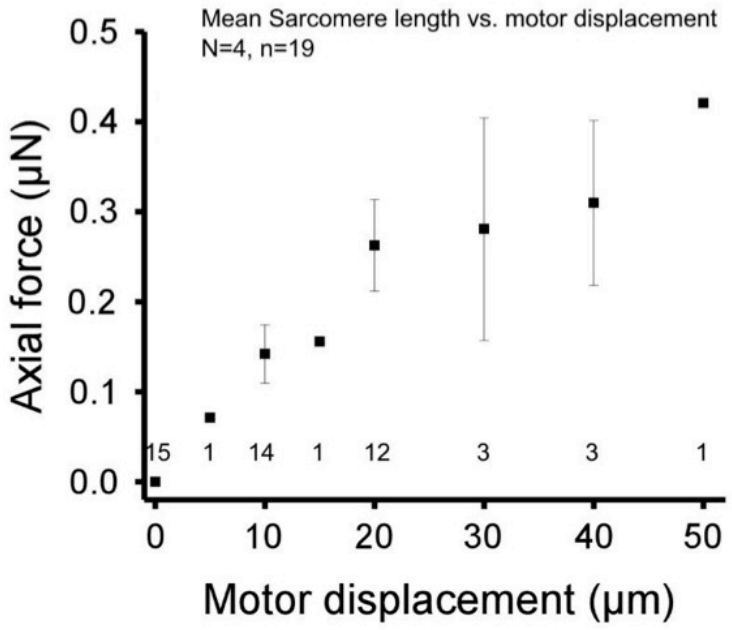

Figure 0.5: Passive axial force versus motor displacement. As anticipated, measured axial force increased with increasing motor displacement. N = 4 mice, n = 19 cells.

Change in cell stiffness in response to stretch

Figure **0**.**7** (A) shows all the three probes aligned on a single isolated adult rat cardiomyocyte. Figure **0**.**7** (B,C,D) represent trends observed on a single cell. It was also confirmed that the change in CF position with motor did result in stretching cell as seen by increase in sarcomere length. At each stretch applied to the cell, AFM cytoindentation was performed to measure elastic modulus of the cell. Our results indicate that radial stretch increases the apparent axial elastic modulus of ventricular cardiomyocytes significantly. Modulus along an individual cell was fairly uniform; no statistical significant difference in AFM data was observed on replicate indentations at same cellular location on each cardiomyocyte. The elastic modulus of cells increased linearly with increase in their sarcomere length. The results show that applying mechanical load on single cells axially results in increase in stiffness of the cell radially.

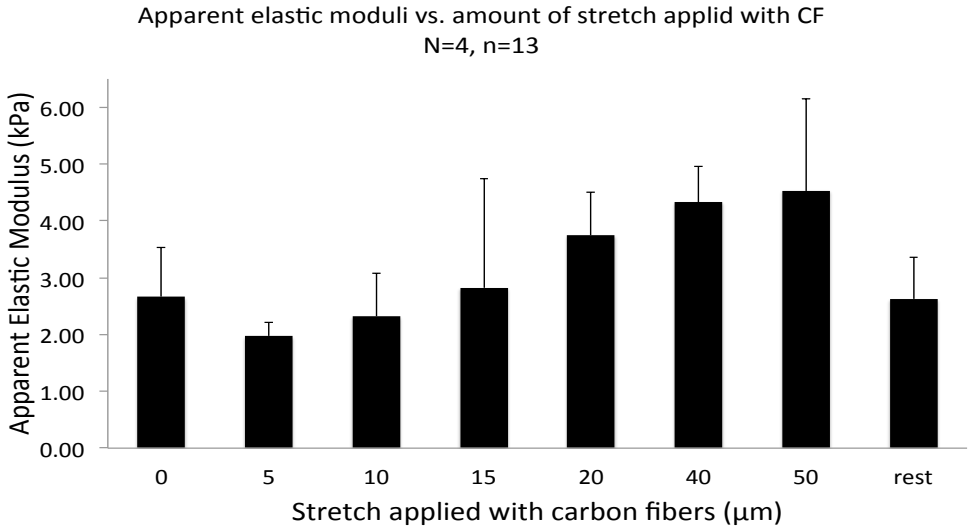

Figure 0.6: Change in apparent elastic modulus of cells in response to stretch. An increase in stiffness (E) of cardiomyocytes is observed as they are stretched axially. N = 4 mice, n = 13 cells.

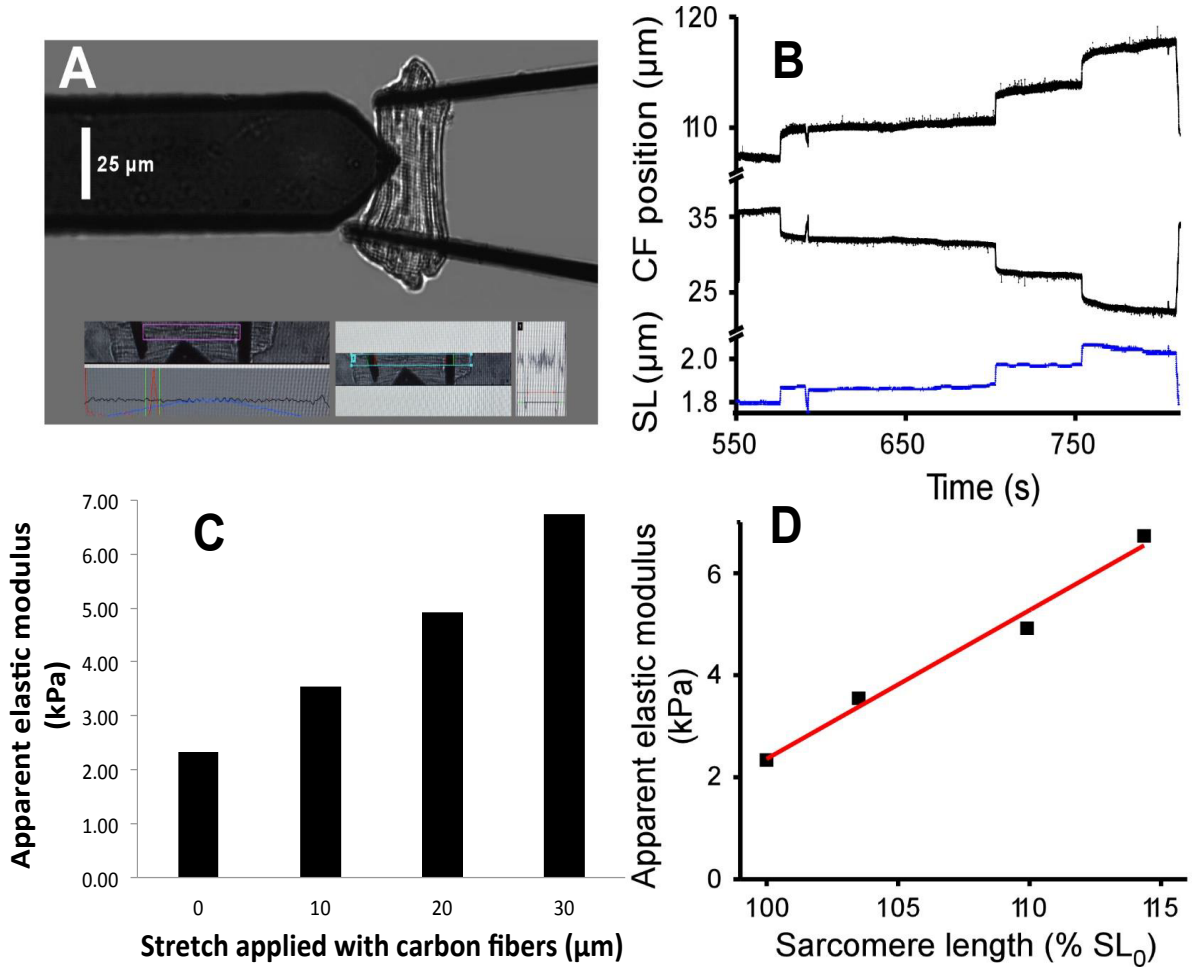

Figure 0.7: Data analysis on a single cardiomyocyte. Apparent elastic modulus is increased by stretch (n=1, external $[Ca^{2+}]$=1.0 mM). (A) A single ventricular cardiomyocyte held by CF under the AFM cantilever. Insets show the contrast based sarcomere and CF detection using the Ion Wizard software developed by IonOptix. (B) CF displacement (black) increasing sarcomere length (blue) overtime. (C) Apparent elastic modulus as measured by AFM vs. stretch applied by carbon fibers. (D) Apparent elastic modulus versus sarcomere length expressed as a percentage of the sarcomere length at rest.

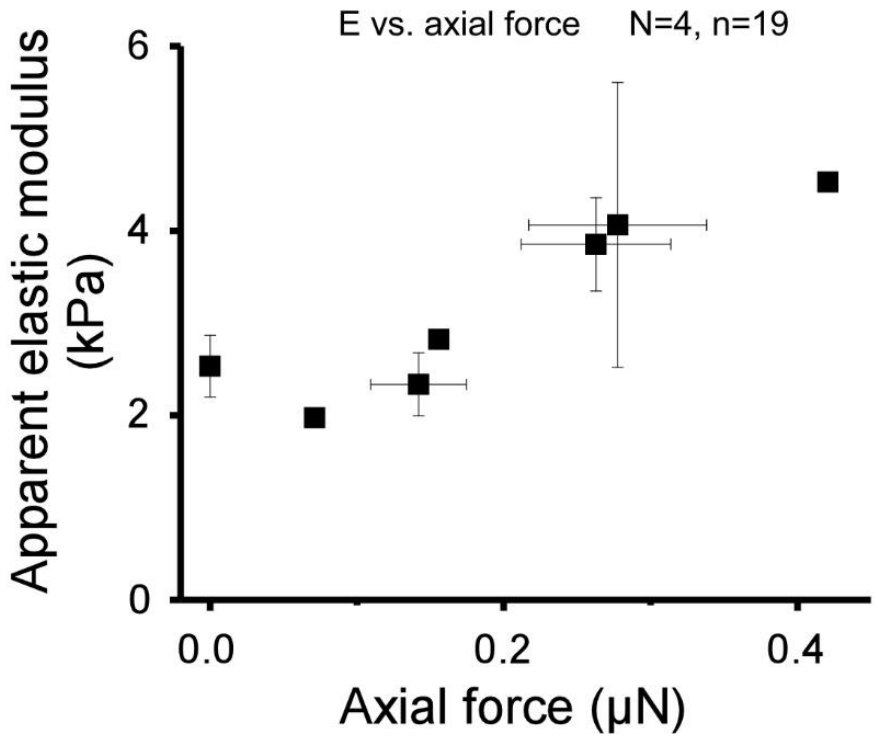

Figure 0.8: Change in axial stiffness of cells in response to applied axial force. N = 4 mice, n = 19 cells.

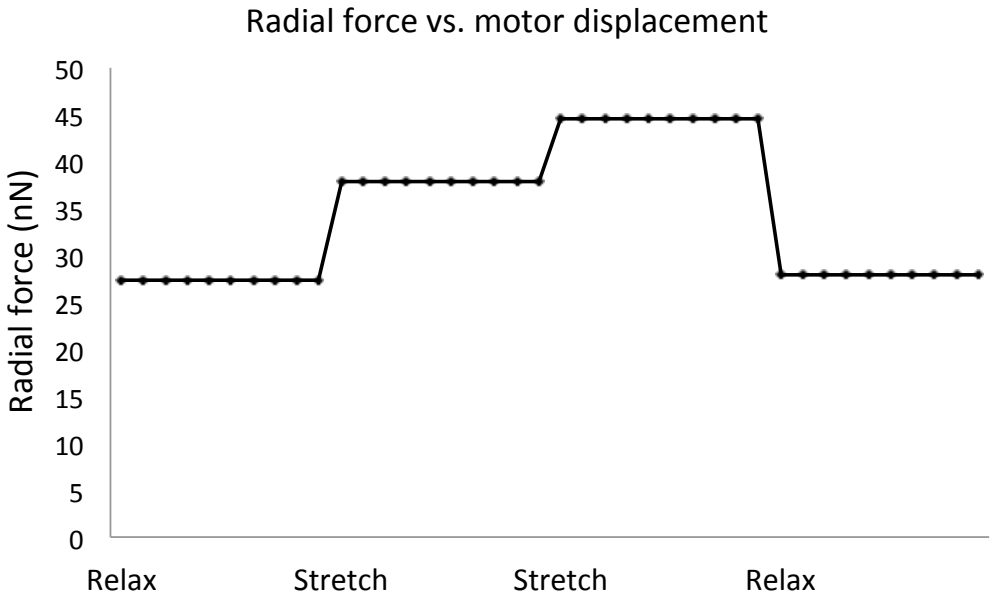

Figure 0.9: Change in radial force in response to stretch. Radial force as measured by AFM versus stretch applied by CF as observed by motor displacement.

Discussion and conclusion

In this study, we have successful at establishing a novel, multidimensional and multimodal technique to study single cell mechanics. We combined two different techniques of single cell mechanics measurements, AFM and CF, in same set up to allow measurement of multidimensional cell mechanics simultaneously.

Indentation testing is an established method to determine samples material properties (33). AFM allows measuring mechanical properties of living cardiomyocytes with nanoscale resolution in transverse direction (30). So, we used this technique to examine potential changes in stiffness and forces on individual isolated cardiomyocytes in radial direction as mechanical load was applied simultaneously in axial direction. Carbon fibers can attach to the cells without disrupting the cell membrane, due to electrostatic forces between the CF surface and the myocyte surfaces (34, 35). We confirmed that as cells are stretched axially with CF's, cellular force increases both axially and radially as measured by CF's and AFM respectively. An increase in apparent elastic modulus of cells (stiffness) is also seen to have increased as they are being stretched.

This new approach of characterizing cell mechanics gives a detailed picture of the balance between axial and radial forces in intact heart muscle cells at rest, during stretch, and in contraction. This will provide new insight to better understand force generation at cell and tissue levels. In addition to being able to combine AFM with CF, the new modified AFM can be coupled with other techniques as well due to wide frontal access. It can be combined with fluorescence microscopy, which will allow studying optogenetics

along with cell mechanics. It will also allow for study of ion channel activity along with mechanics by fitting patch clamp set up along with AFM.

1.22 References

1. Bao G, Suresh S. Cell and molecular mechanics of biological materials. Nature materials. 2003;2(11):715-25.

2. Janmey PA, Miller RT. Mechanisms of mechanical signaling in development and disease. J Cell Sci. 2011 Jan 1;124(Pt 1):9-18.

3. Haase K, Pelling AE. Investigating cell mechanics with atomic force microscopy. J R Soc Interface. 2015 Mar 6;12(104):20140970.

4. Buxboim A, Ivanovska IL, Discher DE. Matrix elasticity, cytoskeletal forces and physics of the nucleus: how deeply do cells 'feel' outside and in? J Cell Sci. 2010 Feb 1;123(Pt 3):297-308.

5. Guolla L, Bertrand M, Haase K, Pelling AE. Force transduction and strain dynamics in actin stress fibres in response to nanonewton forces. J Cell Sci. 2012 Feb 1;125(Pt 3):603-13.

6. Pravincumar P, Bader DL, Knight MM. Viscoelastic cell mechanics and actin remodelling are dependent on the rate of applied pressure. PLoS One. 2012;7(9):e43938.

7. Bufi N, Durand-Smet P, Asnacios A. Single-cell mechanics: the parallel plates technique. Methods Cell Biol. 2015;125:187-209.

8. Suresh S. Biomechanics and biophysics of cancer cells. Acta Materialia. 2007;55(12):3989-4014.

9. Hochmuth RM. Micropipette aspiration of living cells. J Biomech. 2000;33(1):15-22.

10. Fabry B, Maksym GN, Butler JP, Glogauer M, Navajas D, Fredberg JJ. Scaling the microrheology of living cells. Phys Rev Lett. 2001;87(14):148102.

11. Guck J, Schinkinger S, Lincoln B, Wottawah F, Ebert S, Romeyke M, et al. Optical deformability as an inherent cell marker for testing malignant transformation and metastatic competence. Biophys J. 2005;88(5):3689-98.

12. Munevar S, Wang Y, Dembo M. Traction force microscopy of migrating normal and H-ras transformed 3T3 fibroblasts. Biophys J. 2001;80(4):1744-57.

13. Tan JL, Tien J, Pirone DM, Gray DS, Bhadriraju K, Chen CS. Cells lying on a bed of microneedles: an approach to isolate mechanical force. Proc Natl Acad Sci U S A. 2003 Feb 18;100(4):1484-9.

14. Balland M, Richert A, Gallet F. The dissipative contribution of myosin II in the cytoskeleton dynamics of myoblasts. European Biophysics Journal. 2005;34(3):255-61.

15. Allioux-Guerin M, Icard-Arcizet D, Durieux C, Hénon S, Gallet F, Mevel J, et al. Spatiotemporal analysis of cell response to a rigidity gradient: a quantitative study using multiple optical tweezers. Biophys J. 2009;96(1):238-47.

16. Alcaraz J, Buscemi L, Grabulosa M, Trepat X, Fabry B, Farré R, et al. Microrheology of human lung epithelial cells measured by atomic force microscopy. Biophys J. 2003;84(3):2071-9.

17. Webster KD, Crow A, Fletcher DA. An AFM-based stiffness clamp for dynamic control of rigidity. PLoS One. 2011;6(3):e17807.

18. Iribe G, Ward CW, Camelliti P, Bollensdorff C, Mason F, Burton RA, et al. Axial stretch of rat single ventricular cardiomyocytes causes an acute and transient increase in Ca2+ spark rate. Circ Res. 2009 Mar 27;104(6):787-95.

19. Sugiura S, Nishimura S, Yasuda S, Hosoya Y, Katoh K. Carbon fiber technique for the investigation of single-cell mechanics in intact cardiac myocytes. Nature protocols. 2006;1(3):1453-7.

20. Desprat N, Guiroy A, Asnacios A. Microplates-based rheometer for a single living cell. Rev Sci Instrum. 2006;77(5):055111.

21. Mitrossilis D, Fouchard J, Guiroy A, Desprat N, Rodriguez N, Fabry B, et al. Single-cell response to stiffness exhibits muscle-like behavior. Proc Natl Acad Sci U S A. 2009 Oct 27;106(43):18243-8.

22. Silberberg YR, Pelling AE, Yakubov GE, Crum WR, Hawkes DJ, Horton MA. Mitochondrial displacements in response to nanomechanical forces. Journal of Molecular Recognition. 2008;21(1):30-6.

23. Charras GT, Horton MA. Single cell mechanotransduction and its modulation analyzed by atomic force microscope indentation. Biophys J. 2002;82(6):2970-81.

24. Moeendarbary E, Valon L, Fritzsche M, Harris AR, Moulding DA, Thrasher AJ, et al. The cytoplasm of living cells behaves as a poroelastic material. Nature materials. 2013;12(3):253-61.

25. Darling EM, Topel M, Zauscher S, Vail TP, Guilak F. Viscoelastic properties of human mesenchymally-derived stem cells and primary osteoblasts, chondrocytes, and adipocytes. J Biomech. 2008;41(2):454-64.

26. Kuznetsova TG, Starodubtseva MN, Yegorenkov NI, Chizhik SA, Zhdanov RI. Atomic force microscopy probing of cell elasticity. Micron. 2007;38(8):824-33.

27. Li Q, Lee G, Ong C, Lim C. AFM indentation study of breast cancer cells. Biochem Biophys Res Commun. 2008;374(4):609-13.

28. Sader JE, Sanelli JA, Adamson BD, Monty JP, Wei X, Crawford SA, et al. Spring constant calibration of atomic force microscope cantilevers of arbitrary shape. Rev Sci Instrum. 2012;83(10):103705.

29. Mathur AB, Collinsworth AM, Reichert WM, Kraus WE, Truskey GA. Endothelial, cardiac muscle and skeletal muscle exhibit different viscous and elastic properties as determined by atomic force microscopy. J Biomech. 2001;34(12):1545-53.

30. Lieber SC, Aubry N, Pain J, Diaz G, Kim SJ, Vatner SF. Aging increases stiffness of cardiac myocytes measured by atomic force microscopy nanoindentation. Am J Physiol Heart Circ Physiol. 2004 Aug;287(2):H645-51.

31. Collinsworth AM, Zhang S, Kraus WE, Truskey GA. Apparent elastic modulus and hysteresis of skeletal muscle cells throughout differentiation. Am J Physiol Cell Physiol. 2002 Oct;283(4):C1219-27.

32. Costa K, Yin F. Analysis of indentation: implications for measuring mechanical properties with atomic force microscopy. J Biomech Eng. 1999;121(5):462-71.

33. Karduna AR, Halperin HR, Yin FC. Experimental and numerical analyses of indentation in finite-sized isotropic and anisotropic rubber-like materials. Ann Biomed Eng. 1997;25(6):1009-16.

34. Garnier D. Attachment procedures for mechanical manipulation of isolated cardiac myocytes: a challenge. Cardiovasc Res. 1994 Dec;28(12):1758-64.

35. Yasuda SI, Sugiura S, Kobayakawa N, Fujita H, Yamashita H, Katoh K, et al. A novel method to study contraction characteristics of a single cardiac myocyte using carbon fibers. Am J Physiol Heart Circ Physiol. 2001 Sep;281(3):H1442-6.

CHAPTER SIX

CONCLUSIONS AND RECOMMENDATIONS

1.23 Conclusions and discussion

First part of this project involved studying cell mechanics in multidimensional system involving multiple modes of cellular interactions. We were successful at forming microtissues with two different cell types, cardiomyocytes and vascular smooth muscle cells. These provided us with a better model to mimic cellular microenvironment compared to traditional adherent cell culture. Our preliminary studies on cardiomyocyte microtissue culture model also involved use of fibroblast inhibitor cytosine arabinoside (AraC). AFM indentation and SEM analysis of microtissues with and without AraC revealed that AraC does interfere with the mechanics of CM. A significant drop in the apparent elastic modulus was observed on the cells with the inhibitor. SEM imaging also showed distinct difference in the roughness of the microtissues with AraC.

Also, effects of cell-cell and cell-matrix interactions on mechanics (stiffness) of cells were studied. Specific cellular interactions were blocked individually and in combination using antibodies and AFM mechanical studies were performed. This was the first study to investigate role of integrin β1, connexins 43, and N-cadherin mediated cellular interactions on mechanical properties of cardiovascular cells in scaffold free 3D culture system.

Our results from cell-cell and cell-matrix interactions individually and in combination indicate significant drop in cellular stiffness in cardiac microtissues.

However, the results from VSMC microtissues do not follow the same trend. VSMC studies show and increase in cellular stiffness by blocking cell-cell interactions. Interestingly, our results from blocking studies in microtissue follow similar trends to the blocking studies on 2D, adherent culture previously done in our lab. Blocking studies in 2D have resulted in elastic moduli ranging from 2.3 kPa to 5.3 kPa under experimental conditions, a significant drop compared to no antibody (8.6 kPa) and IgG (10.6 kPa) control conditions. Increase in stiffness of VSMCs spheroids on blocking N-cadherin interactions have been consistent with previous studies done in our lab in on VSMCs cultured on polyacrylamide gels, Charras et.al. (1) observed similar results by blocking E-cadherin interactions on epithelial cells on collagen gels.

Tissue elasticity is a highly regulated determinant of normal tissue development and function. Several studies have shown progressive stiffening on the extracellular matrix (ECM) in diseases including but not limited to cancer, cirrhosis, pulmonary fibrosis, and vascular diseases. Cell-cell and cell-ECM interactions are dynamic sites of chemical and mechanical stimuli that govern multiple phenomena, including cell sorting, wound healing, and tissue reorganization. Previous studies involving inhibition of cell-cell and cell-matrix interactions have focused on studying the effects of blocking on cell proliferation, migration, differentiation, adhesion, disease progression, and apoptosis (2-8). However, through this study, we were for the first time able to study effects of cell-cell and cell-matrix interactions on the scaffold free 3D culture system, enabling more in vivo like environment.

Our results indicate that cell stiffness changes under antibody blocking conditions in both cardiomyocyte as well as smooth muscle cells. Blocking cell-matrix interactions of integrin β1 results in decrease in stiffness of cells. However, blocking cell-cell interactions of connexin 43 in CMs results in less stiff less, whereas N-cadherin blocking in VSMCs results in significantly stiffer cells. Elastic modulus values suggest that integrin β1, connexins 43, and N-cadherin play an important role in determining cellular mechanical properties. The influence of connexin 43 and N-cadherin mediated cell-cell interactions and integrin β1 mediated cell-matrix interactions on elastic modulus of cellular microtissues were assessed for the first time in this study. Blocking these interactions individually and in combination resulted in reduced cellular elastic modulus in both CMs and SMCs (except anti N-cadherin media condition).

These results provide researchers with better understanding of the role of cellular adhesions in regulating mechanical properties at tissue scale.

Second part of the project involved studying mechanics of a single cell in multiple dimensions via. multiple modes of measurement. We were successful at establishing a novel, multidimensional and multimodal technique to study single cell mechanics. Two different techniques of single cell mechanics measurements, AFM and CF, were combined under a single set up to allow measurement of both radial and axial cell mechanics simultaneously.

Indentation testing is an established method to determine samples material properties. AFM allows measuring mechanical properties of living cardiomyocytes with nanoscale resolution in transverse direction. So, we used this technique to examine

potential changes in stiffness and forces on individual isolated cardiomyocytes in radial direction as mechanical load was applied simultaneously in axial direction. Carbon fibers can attach to the cells without disrupting the cell membrane, due to electrostatic forces between the CF surface and the myocyte surfaces. We confirmed that as cells are stretched axially with CF's, cellular force increases both axially and radially as measured by CF's and AFM respectively. An increase in apparent elastic modulus of cells (stiffness) is also seen to have increased as they are being stretched.

In addition, active and passive forces during rest and contracture on single cardiomyocytes were also measured. One of the important results from this study shows that every time axial stretch is applied with CF a corresponding increase in stiffness and force was measured in radial direction as measured by AFM. The forces and stiffness measured before and after the application of stretch were similar showing the elastic behavior of these important cells of heart.

This new approach of characterizing cell mechanics gives a detailed picture of the balance between axial and radial forces in intact heart muscle cells at rest, during stretch, and in contraction. This will provide new insight to better understand force generation at cell and tissue levels.

1.24 Recommendations for future work

Quantitative analysis of microtissues

In cellular blocking studies (chapter 4) we performed ImageJ analysis of different microtissue to study phenotypic changes and mechanically probed them to measure their

stiffness. In order to quantitatively prove cellular blocking, immunofluorescence imaging needs to be performed. We already have a protocol optimized for staining spheroids, which will be used to perform these experiments. Further histology on spheroids needs to be performed to examine the variations in matrix production under different antibody conditions.

Co-culture of cells in microtissue

The overall goal is to develop a tissue to organ level computational model that can predict response to mechanical stimuli in vivo. The model will be based on experimental studies performed at single cell and microtissue scale. In this study (chapter 4), we studied effects of blocking cellular interactions on its mechanics in cardiomyocyte and vascular smooth muscle cell microtissue models. However, cardiovascular system involves a wide array of additional cell types including but not limited to endothelial cells, fibroblasts, immune cells, mast cells, etc. In order to gain a better understanding of the affects of interactions of different cell types at tissue level, a co-culture of spheroids will be an ideal system.

AFM-CF studies on diseased cells

In order to develop a tissue level model that incorporates mechanics observed at single cell level would require understanding of both healthy and diseased states. In chapter 5, we studied both radial and axial mechanics of a single adult cardiomyocyte from a healthy mice hearts. Replicating these studies on cells from diseased heart would

help better compare and understand the differences in the stiffness and forces in healthy versus diseased.

Different set ups with modified AFM

In addition to being able to combine AFM with CF, the new modified AFM can be coupled with other techniques also due to wide frontal access. It can be combined with fluorescence microscopy, which will allow studying optogenetics along with cell mechanics. Optogenetics is a method that uses light to modulate molecular events in a targeted manner in living cells or organisms. It relies on the use of genetically encoded proteins that change conformation in the presence of light to alter cell behavior (9). The new modified AFM will also allow for the study of ion channel activity along with mechanics by fitting patch clamp set up with AFM. This will allow for the measurement of both mechanical and electrical response of cells to loading.

Create tissue level mechanical models

This work provided insights into the cellular mechanics in multiple dimensions at both single cells as well microtissue level. The ultimate fulfillment of this work would be its incorporation into a multiscale model, leading to the ability to tie macro- scale behaviors to nano- scale phenomenon. A finite element model of at tissue level that is based of from experimental data would be ideal. Such a model could potentially be used in drug development, tissue engineering, and regenerative medicine therapies, thereby possibly increasing the quality and longevity of lives in future.

1.25 References

1. Harris AR, Daeden A, Charras GT. Formation of adherens junctions leads to the emergence of a tissue-level tension in epithelial monolayers. J Cell Sci. 2014 Jun 1;127(Pt 11):2507-17.

2. Koutsouki E, Beeching CA, Slater SC, Blaschuk OW, Sala-Newby GB, George SJ. N-cadherin-dependent cell-cell contacts promote human saphenous vein smooth muscle cell survival. Arterioscler Thromb Vasc Biol. 2005 May;25(5):982-8.

3. McNally AK, Anderson JM. β1 and β2 integrins mediate adhesion during macrophage fusion and multinucleated foreign body giant cell formation. The American journal of pathology. 2002;160(2):621-30.

4. Hermiston ML, Gordon JI. In vivo analysis of cadherin function in the mouse intestinal epithelium: essential roles in adhesion, maintenance of differentiation, and regulation of programmed cell death. J Cell Biol. 1995 Apr;129(2):489-506.

5. Steinberg MS, McNutt PM. Cadherins and their connections: adhesion junctions have broader functions. Curr Opin Cell Biol. 1999;11(5):554-60.

6. Li G, Satyamoorthy K, Herlyn M. N-cadherin-mediated intercellular interactions promote survival and migration of melanoma cells. Cancer Res. 2001 May 1;61(9):3819-25.

7. Cheng S, Shin CS, Towler DA, Civitelli R. A dominant negative cadherin inhibits osteoblast differentiation. Journal of Bone and Mineral Research. 2000;15(12):2362-70.

8. Siebers M, Walboomers X, van den Dolder J, Leeuwenburgh S, Wolke J, Jansen J. The behavior of osteoblast-like cells on various substrates with functional blocking of integrin-β1 and integrin-β3. J Mater Sci Mater Med. 2008;19(2):861-8.

9. Vogt N. Precision optogenetics. Nature Methods. 2016;13(1):34-.

APPENDICES

Appendix A

Vascular Smooth Muscle Cell Isolation Protocol

Aortic VSMCs were isolated from week 12 Sprague-Dawley rats via the following protocol [1]. The rats were first euthanized by carbon dioxide asphyxiation. The abdomen was split longitudinally from the pelvis to the clavicle. The internal organs were dissected away to expose the aorta along the posterior abdominal wall. The aorta was then clipped at the pelvic bifurcation and dissected away from the dorsal abdominal wall to the aortic arch. Approximately 3 ml of cold transport medium (Dulbecco's Modified Eagle's Medium (DMEM, Fisher Scientific, Pittsburgh, PA, USA) + 100 μg/ml penicillin/streptomycin (Sigma-Aldrich, St. Louis, MO, USA) + 2 μg/ml fungizone (Sigma-Aldrich)) was used to flush the aorta via hypodermic injection through the wall of the left ventricle. The aorta was then clipped at the aortic arch and placed in cold transport medium for transport from the animal facility to the lab. Next, excess fat and the adventitial layer of the artery were peeled away, in the presence of PBS to prevent drying and to maintain cell viability. Arterioles were then trimmed away and the aortic segments split lengthwise and laid open with the intima facing up. A sterile scalpel was used to scrape away the endothelial layer of the vessel. The aortic segments were then rinsed in PBS to remove any loose cells on the surface. Sterile scissors were used, under magnification, to finely mince the segments into approximately 0.5 mm pieces. The minced artery segments were placed in 15 ml tubes, each containing 10 ml of a DMEM/protease digestion solution (10 ml DMEM + 10 mg collagenase type II (Worthington Biochemical, Lakewood, NJ, USA) + 2.5 mg elastase (Worthington

Biochemical) + 1.5 mg soybean trypsin inhibitor (Worthington Biochemical)). The 15 ml tubes were placed in an incubator for 20-25 minutes at 37ºC and 5% carbon dioxide with mixing (gently inverting tubes 2-3 times) every 5 minutes. The aortic segments settled at the bottom of the tubes and the digestion solution was then aspirated. Next, the segments were resuspended in 10 ml of vascular smooth muscle cell (VSMC) media (DMEM + 10% FBS (Sigma-Aldrich) + 1% antibiotic/antimycotic solution (Sigma-Aldrich)) to dilute and deactivate the digestion solution. A sterile scalpel blade was then used to lightly scratch a small asterisk shaped pattern on the bottom of each well in a six well plate to aid in the adhesion of the tissue segments. Four arterial segments were placed in each well directly atop the scratched pattern, with a single drop of VSMC media to keep them moist and viable without allowing them to move from the scratched surface. The plates were incubated for 24 hours to allow for adhesion and then supplemented with 1.5 ml additional media, being careful not to dislodge the attached tissue. The plates were incubated for the next 7 to 10 days (until cells could be seen growing away from the tissue segments in several patches), with media changes every 48 hours. When the patches of adherent cells reached confluence, the tissue segments were carefully removed and the cells passaged and cultured with 12 ml media in T75 flasks.

Appendix B

MATLAB Scripts (Chapter 4 data analysis)

Example of what to call in command window:

e = massexcompile('Day 5 VSMC') (folder containing exported data)

Scripts:

massexcompile.m

- Loads raw AFM force-indentation data

```
function [elasticity Curves] = massexcompile(folderin)
% folderin should be the folder your data is in. something like "C:\Documents and
Setting\My Documents\MyData"
mainfolder = cd
format long
fnames = dir(folderin);
numfids = length(fnames);
cd(folderin);
%filtering out irrelevent "files" such as '.' and '..'
cellnames = {};
for s = 1:numfids;
   if 'c' == fnames(s).name(1) % 'c' represents the letter that the relevent file names begin
with
      cellnames{end+1} = fnames(s).name;
```

```
    end
end
%combine every 3 files and write
counter = 1;
numcell = length(cellnames);
numfile = 1;
elasticity = [];
% OMIT THIS WHILE LOOP IF YOU WANT TO LOAD CELLS INDIVIDUALLY
Curves(numcell, 1) = struct('extension', [], 'retraction', []);
CurrentCell =1;
while counter <= numcell
    a = load(cellnames{counter});
    c = load(cellnames{counter+2});
    cd(mainfolder);
    [elasticity(end+1,1) xe ye xr yr] = elast_analysis(c,a,mainfolder,counter);
    Curves(CurrentCell).extension = [xe ye];
    Curves(CurrentCell).retraction = [xr yr];
    %figure('Name',sprintf('Cell %d', ((counter-1)/3)+1),'NumberTitle','off')  %comment
out in order to turn plotting off
    %plot(c,a)              %comment out in order to turn plotting off
    counter = counter+3;
    CurrentCell = CurrentCell+1;
```

```
    cd(folderin);
    %numfile = numfile+1
end
cd(mainfolder)
```

elast_analysis.m

- Fits Hertz model to force-indentation data and outputs apparent elastic modulus measures in Pascals for each indentation file in input folder
- Calls AFM_butter.m and xycorrect.m scripts

```
function [e xe ye xr yr] = elast_analysis(c,a,mainfolder,counter)
cd(mainfolder)
format long
k = 0.12; %spring constant value N/m
v = 0.5; %poisson's ratio
R = 2.5*10^-6;  % tip radius in meters
L = 30*10^-9 ;     %lower bound for elasticity (in m from contact point)
U = 300*10^-9 ;   %upper bound for elasticity (in m from contact point)
%adjust deflection
ak = a;
%filter deflection values
d = AFM_butter(ak);
%Separation of extension and retraction
l = floor(length(c)/2);
```

```
xe = c(200:l);% add 200 in order to omit first several data points (irratic behavior due to
filtering
ye = d(200:l);
if rem(length(c),2)==0;
   xr = c(end-200:-1:l+1); % subtract 200 in order to omit first several data points
   yr = d(end-200:-1:l+1);
   else
   xr = c(end-200:-1:l+2);
   yr = d(end-200:-1:l+2);
end
%correct x,y offsets
[xe,ye] = xycorrect(xe,ye);
[xr,yr] = xycorrect(xr,yr);
ye = k * ye;
yr = k * yr;
format long;
erange = [];
for i = [1:1:length(xe)];
   if xe(i)>=L && xe(i)<=U;
      erange(end+1) = i;
   end;
end;
```

```
rrange = [];
for i = [1:1:length(xr)];
   if xr(i)>=L && xr(i)<=U;
      rrange(end+1) = i;
   end;
end;
emodulus = mean((3.*ye(erange).*(1-v^2))./(4.*xe(erange).^(3/2).*R.^(1/2)));
%rmodulus = mean((3.*yr(rrange).*(1-v^2))./(4.*xr(rrange).^(3/2).*R.^(1/2)));
figure('Name',sprintf('Sample %d', ((counter-1)/3)+1),'NumberTitle','off')
plot(xe,ye)
hold on
plot(xe(erange),ye(erange),'r')
e = [emodulus];
```

AFM_butter.m

Applies Butterworth filter to data

```
function [i] = AFM_butter(x) %applies butterworth filter to data
format long
[b,a]=butter(3,.025);
i=filter(b,a,x);
```

xycorrect.m

Corrects x and y offsets in data to set contact point to (0,0)

```
function [xc,yc] = xycorrect(x,y)
s = 0.008; %slope sensitivity
%correction for y
format long
region = [1:length(x)/4];
slope = polyfit(x(region),y(region),1);
yci = y-(polyval(slope, x));
%correction for x
numslope = diff(yci)./diff(x);
index = 1;
condition = 0;
contactx = 0
while condition == 0 && index ~= length(numslope)
   if numslope(index) > s && mean(numslope(index:5:index+200)) > s;
      condition = 1;
      contactx = index;
   end
   index = index+1;
end
xc = x-x(contactx)-yci;
% correct again for y
yc = yci-yci(contactx);
```

Appendix C

MATLAB Scripts (Chapter 5 data analysis)

ImportAFMWorkshopForces.m

```
function [RawData] = ImportAFMWorkshopForces(DirectoryName)
% function [RawData] = ImportAFMWorkshopForces(DirectoryName)
% For converting and analyzing AFM data from the AFMWorkshop machine, start with
this function! Then you can use, ConvertAFMWorkshop to do the rest of the data
conversion and analysis. This function reads in the data from the AFM .csv raw data files.
% DirectoryName is the string representing the directory where the data files are located.
% The data will be imported into RawData. This will be a structure with fields for the
File name, directory name, raw data, etc.
% Please see the function ConvertAFMWorkshopForce.m for more information on what
to do next.
FileNames = dir(DirectoryName);
NumFiles = length(FileNames);
RawData = struct('FileName', {}, 'DirectoryName', {}, 'RawData', {}, 'k', {}, 'DefSens',
{}, 'Rtip', {}, 'ConvertedData', {}, 'Modulus', {}, 'ModulusStd', {}, 'Hysteresis', {},
'PointByPointE', {});
% Mac = input('is this a Mac? yes or no ', 's');
Mac = strfind(DirectoryName, '/');
Mac = sum(Mac) >0;
```

```
NonDataFileCounter = 0;
for i = 1:NumFiles,
   LengthName = length(FileNames(i).name);
   if LengthName>3
      if (FileNames(i).isdir == 0) && strcmp(FileNames(i).name(LengthName-
3:LengthName), '.csv')
         if strcmp(Mac, 'yes')
            CurFile = strcat(DirectoryName, '/', FileNames(i).name);
         else
            CurFile = strcat(DirectoryName, '\', FileNames(i).name);
         end
         CurData = importdata(CurFile, ',', 4); % assumes 4 lines of header and
delimination with ','
         RawData(i-NonDataFileCounter).FileName = FileNames(i);
         RawData(i-NonDataFileCounter).DirectoryName = DirectoryName;
         RawData(i-NonDataFileCounter).RawData = CurData.data;
      else
         NonDataFileCounter = NonDataFileCounter+1;
      end
   else
      NonDataFileCounter = NonDataFileCounter+1;
   end
```

```
end
```

ConvertAFMWorkshopForce.m

```
function [DataStructure] = ConvertAFMWorkshopForce(InDataStructure, varargin)
DataStructure = InDataStructure;
NumberOfExtraInputs = length(varargin);
NumDataSets = length(DataStructure);
prompt = 1;
Ramp = 0;
CurDefSens = DataStructure(1).DefSens;
CurK = DataStructure(1).k;
if isempty(CurK),
   CurK = input('Enter the spring constant in N/m: ');
end
if isempty(DataStructure(1).Rtip)
   Rtip = input('Enter the tip radius in nm: ');
end
DataConvPrompt = input('Do you want to convert your raw data to force-distance
curves? (yes or no) ', 's');
if strcmp(DataConvPrompt, 'yes')
   for i =1:NumDataSets,
      disp('Processing file: ')
      DataStructure(i).FileName.name
```

```
[m n] = size(DataStructure(i).RawData);
if isempty(CurDefSens)&&isempty(DataStructure(i).DefSens),
    disp('What is the deflection sensitivity (in nm/V)? if unknown, please')
    disp('enter 0 and I will assume that this is a calibration data on a ')
    CurDefSens = input('hard substrate and use the first data set to calculate it  ');
elseif isempty(DataStructure(i).DefSens)
    DataStructure(i).DefSens = CurDefSens;
else
    CurDefSens = DataStructure(i).DefSens;
end
if isempty(DataStructure(i).k)
    DataStructure(i).k = CurK;
end
if isempty(DataStructure(i).Rtip)
    DataStructure(i).Rtip = Rtip;
end
if n ==2 && prompt,
    Ramp = input('What is the size of the ramp used for this data? (in nm) ');
    PAns = input('Is the ramp size for every file the same? (yes or no) ', 's');
    prompt = strcmp(PAns, 'no');
end
if n ==2,
```

```
        [DataStructure(i).ConvertedData,  DataStructure(i).DefSens] =
ConvertAFMWorkshopOldForce(DataStructure(i).RawData, Ramp, CurDefSens,
DataStructure(i).k);
      else
        [DataStructure(i).ConvertedData,  DataStructure(i).DefSens] =
ConvertAFMWorkshopNewForce(DataStructure(i).RawData, CurDefSens,
DataStructure(i).k);
      end
   end
end
DataAnalysisPrompt = input('Do you want to analyze your curves to get modulus values?
(yes or no) ', 's');
if strcmp(DataAnalysisPrompt, 'yes')
   for i = 1:NumDataSets,
      [DataStructure(i).Modulus, DataStructure(i).ModulusStd,
DataStructure(i).Hysteresis, DataStructure(i).PointByPointE] =
AnalyzeForceCurveAFMWorkshop(DataStructure(i).ConvertedData,
DataStructure(i).Rtip);
   end
end
```

ConvertAFMWorkshopNewForce.m

```
function [ConvertedData, DefSens] = ConvertAFMWorkshopNewForce(RawData,
DefSens, SpringConstant)
disp('Length of data is: ')
NumDataPoints = ( length(RawData(:, 1)))
RawData = RawData(1:NumDataPoints, :);
% Assume a linear approach on Z and use the RampSize as the range
ZApproach = RawData(:, 1)- RawData(1,1);
ZRetract = RawData(:, 3)- RawData(1, 3);
figure
plot(ZApproach, RawData(:, 2))
IsIndent = input('Is this indentation data? (default is yes) ', 's');
if isempty(IsIndent)
   IsIndent = 'yes';
end
disp('I will remove the baseline ofset. If you do not enter values, I will use the program
defaults.\n')
MinX = input('what is the minimum x value on the graph that you consider baseline? ');
MaxX = input('what is the maximum x value on the graph that you consider basline? ');
CurrentPosition = NumDataPoints;
BeginFlag = 1; %BeginFlag is 0 when you have found the beginning position of the
baseline in the data
```

```
EndFlag = 1;  %EndFlag is 0 when you have found the ending position of the baseline in
the data
if isempty(MinX)
    % Remove baseline shift from data. Here we assume that at least the first
    % half of the data is baseline (i.e. the tip is approaching the sample
    % but hasn't touched it yet).
    FractionBaseLine = 1/2; % fraction of data that is baseline
    BeginBaseLine = round(NumDataPoints * FractionBaseLine);
    BeginFlag = 0;
end
if isempty(MaxX)
    EndBaseLine = NumDataPoints;
    EndFlag = 0;
end
while CurrentPosition > 1 && (BeginFlag || EndFlag)
    if ZApproach(CurrentPosition, 1)< MaxX && EndFlag
        EndBaseLine = CurrentPosition;
        EndFlag = 0;
    end
    if ZApproach(CurrentPosition, 1) < MinX && BeginFlag
        BeginBaseLine = CurrentPosition;
        BeginFlag = 0;
```

```
    end
    CurrentPosition = CurrentPosition -1;
end
ZAppFit = ZApproach(BeginBaseLine:EndBaseLine, 1);
RawDataFit = RawData(BeginBaseLine:EndBaseLine, 2);
BaseLineFit = polyfit(ZAppFit, RawDataFit, 1);
% hold on
% plot(ZApproach, RawData(:,1), 'b');
% plot(ZApproach, LinearBaselineFit, 'g');
ConvertedDataForceApproach = RawData(:, 2) - polyval(BaseLineFit, ZApproach);
ConvertedDataForceRetract = RawData(:, 4) - polyval(BaseLineFit, ZRetract);
ConvertedDataForceRetract = ConvertedDataForceRetract -
mean(ConvertedDataForceRetract(NumDataPoints-5:NumDataPoints, 1));

ConvertedData = [ZApproach ConvertedDataForceApproach ZRetract
ConvertedDataForceRetract];

% hold on
% plot(ConvertedData(:, 1), ConvertedData(:, 2), 'b')
% plot(ConvertedData(:, 3), ConvertedData(:, 4), 'r')

if DefSens ==0
```

```
    % calculate the deflection sensitivity if it was not passed in
    % This assumes that the deflection sensistivity is calculated on the
    % part of the data that goes above ThreshVolt of value.
    DefSensPoints = BeginBaseLine;
    Base = mean(ConvertedData(DefSensPoints:EndBaseLine,2));
    CurrentLevelDeflection=Base;
    figure
    plot(ConvertedData(:, 1), ConvertedData(:, 2))
    ThreshVolt = input('Around what y-value on the graph would you like to calculate the
deflection sensitivity? '); %Threshold value (in V) over which you have hit the surface
    if isempty(ThreshVolt)
        disp('I will use the default 0.2 since you did not enter a value')
        ThreshVolt = 0.2;
    end
    while (DefSensPoints>5)&& (CurrentLevelDeflection-Base)<ThreshVolt
        CurrentLevelDeflection = mean(ConvertedData(DefSensPoints-5:DefSensPoints+5,
2));
        DefSensPoints = DefSensPoints-1;
    end
    DefSensPoints
    %hold on
```

```
    %plot(ConvertedData(DefSensPoints-10:DefSensPoints+10, 1),
ConvertedData(DefSensPoints-10:DefSensPoints+10, 2), '.g')
    DefSensFit = polyfit(ConvertedData(DefSensPoints-5:DefSensPoints+5, 1),
ConvertedData(DefSensPoints-5:DefSensPoints+5, 2), 1);
    DefSens = -1/DefSensFit(1)
    %figure
end
% convert the deflection data from V to nm
ConvertedData(:, 2) = ConvertedData(:, 2)*DefSens;
ConvertedData(:, 4) = ConvertedData(:, 4)*DefSens;

% convert Z piezo distance to tip-sample separation
ConvertedData(:, 1) = ConvertedData(:, 1) + ConvertedData(:, 2);
ConvertedData(:, 3) = ConvertedData(:, 3) + ConvertedData(:, 4);

% convert the deflection data from nm to nN
ConvertedData(:, 2) = ConvertedData(:, 2)*SpringConstant;
ConvertedData(:, 4) = ConvertedData(:, 4)*SpringConstant;
BaseLineNoiseLevel = std(ConvertedData(BeginBaseLine:EndBaseLine, 2)); %Level of
noise on the baseline in nN

% find contact point
```

```
ContactPoint = NumDataPoints-5;

while ContactPoint >6 && mean(ConvertedData(ContactPoint-5:ContactPoint+5,
2))<BaseLineNoiseLevel*5
    ContactPoint = ContactPoint-1;
end
ContactDist = ConvertedData(ContactPoint, 1)
ConvertedData(:, 1) = ConvertedData(:, 1)- ContactDist;
ConvertedData(:, 3) = ConvertedData(:, 3) - ContactDist;

if strcmp(IsIndent, 'yes')
    ConvertedData(:, 1) = -ConvertedData(:, 1);
    ConvertedData(:, 3) = -ConvertedData(:, 3);
end
%figure
plot(ConvertedData(:, 1), ConvertedData(:, 2), 'b')
hold on
plot(ConvertedData(:, 3), ConvertedData(:, 4), 'r')
```

ConvertAFMWorkshopOldForce.m

```
function [ConvertedData, DefSens] = ConvertAFMWorkshopOldForce(RawData,
RampSize, DefSens, SpringConstant)
disp('Length of data is: ')
```

```
NumDataPoints = ( length(RawData(:, 1)) - 1) %The last point in the input file is always
a NaN so remove it.
RawData = RawData(1:NumDataPoints, :);

% Assume a linear approach on Z and use the RampSize as the range
ZApproach = linspace(0, RampSize, NumDataPoints)';
ZRetract = ZApproach;

figure
plot(ZApproach, RawData(:, 1))
IsIndent = input('Is this indentation data? (default is yes) ', 's');
if isempty(IsIndent)
    IsIndent = 'yes';
end
disp('I will remove the baseline ofset. If you do not enter values, I will use the program
defaults.\n')
MinX = input('what is the minimum x value on the graph that you consider baseline? ');
MaxX = input('what is the maximum x value on the graph that you consider basline? ');
CurrentPosition = NumDataPoints;
BeginFlag = 1; %BeginFlag is 0 when you have found the beginning position of the
baseline in the data
```

```
EndFlag = 1;  %EndFlag is 0 when you have found the ending position of the baseline in
the data
if isempty(MinX)
    % Remove baseline shift from data. Here we assume that at least the first
    % half of the data is baseline (i.e. the tip is approaching the sample
    % but hasn't touched it yet).
    FractionBaseLine = 1/2; % fraction of data that is baseline
    BeginBaseLine = round(NumDataPoints * FractionBaseLine);
    BeginFlag = 0;
end

if isempty(MaxX)
    EndBaseLine = NumDataPoints;
    EndFlag = 0;
end
while CurrentPosition > 1 && (BeginFlag || EndFlag)
    if ZApproach(CurrentPosition, 1)< MaxX && EndFlag
        EndBaseLine = CurrentPosition;
        EndFlag = 0;
    end
    if ZApproach(CurrentPosition, 1) < MinX && BeginFlag
        BeginBaseLine = CurrentPosition;
```

```
        BeginFlag = 0;
    end
    CurrentPosition = CurrentPosition -1;
end

ZAppFit = ZApproach(BeginBaseLine:EndBaseLine, 1);
RawDataFit = RawData(BeginBaseLine:EndBaseLine, 1);
BaseLineFit = polyfit(ZAppFit, RawDataFit, 1);
% hold on
% plot(ZApproach, RawData(:,1), 'b');
% plot(ZApproach, LinearBaselineFit, 'g');
ConvertedDataForceApproach = RawData(:, 1) - polyval(BaseLineFit, ZApproach);
ConvertedDataForceRetract = RawData(:, 2) - polyval(BaseLineFit, ZRetract);
ConvertedDataForceRetract = ConvertedDataForceRetract -
mean(ConvertedDataForceRetract(NumDataPoints-5:NumDataPoints, 1));

ConvertedData = [ZApproach ConvertedDataForceApproach ZRetract
ConvertedDataForceRetract];

% hold on
% plot(ConvertedData(:, 1), ConvertedData(:, 2), 'b')
% plot(ConvertedData(:, 3), ConvertedData(:, 4), 'r')
```

```
if DefSens ==0
    % calculate the deflection sensitivity if it was not passed in
    % This assumes that the deflection sensistivity is calculated on the
    % part of the data that goes above ThreshVolt of value.
    DefSensPoints = NumDataPoints-10;
    Base = mean(ConvertedData(DefSensPoints:DefSensPoints+10,2));
    CurrentLevelDeflection=Base;
    figure
    plot(ConvertedData(:, 1), ConvertedData(:, 2))
    ThreshVolt = input('Around what y-value on the graph would you like to calculate the
deflection sensitivity? '); %Threshold value (in V) over which you have hit the surface
    if isempty(ThreshVolt)
        disp('I will use the default 0.2 since you did not enter a value')
        ThreshVolt = 0.2;
    end
    while (DefSensPoints>1)&& (CurrentLevelDeflection-Base)<ThreshVolt
        CurrentLevelDeflection = mean(ConvertedData(DefSensPoints:DefSensPoints+10,
2));
        DefSensPoints = DefSensPoints-1;
    end
```

```
    %plot(ConvertedData(DefSensPoints-10:DefSensPoints+10, 1),
ConvertedData(DefSensPoints-10:DefSensPoints+10, 2), '.g')
    DefSensFit = polyfit(ConvertedData(DefSensPoints-10:DefSensPoints+10, 1),
ConvertedData(DefSensPoints-10:DefSensPoints+10, 2), 1);
    DefSens = -1/DefSensFit(1)
end

% convert the deflection data from V to nm
ConvertedData(:, 2) = ConvertedData(:, 2)*DefSens;
ConvertedData(:, 4) = ConvertedData(:, 4)*DefSens;
% convert Z piezo distance to tip-sample separation
ConvertedData(:, 1) = ConvertedData(:, 1) + ConvertedData(:, 2);
ConvertedData(:, 3) = ConvertedData(:, 3) + ConvertedData(:, 4);
% convert the deflection data from nm to nN
ConvertedData(:, 2) = ConvertedData(:, 2)*SpringConstant;
ConvertedData(:, 4) = ConvertedData(:, 4)*SpringConstant;
BaseLineNoiseLevel = std(ConvertedData(BeginBaseLine:EndBaseLine, 2)); %Level of
noise on the baseline in nN
% find contact point
ContactPoint = EndBaseLine;
while ContactPoint >6 && mean(ConvertedData(ContactPoint-5:ContactPoint+5,
2))<BaseLineNoiseLevel*5
```

```
    ContactPoint = ContactPoint-1;
end

ContactDist = ConvertedData(ContactPoint, 1)
ConvertedData(:, 1) = ConvertedData(:, 1)- ContactDist;
ConvertedData(:, 3) = ConvertedData(:, 3) - ContactDist;
if strcmp(IsIndent, 'yes')
    ConvertedData(:, 1) = -ConvertedData(:, 1);
    ConvertedData(:, 3) = -ConvertedData(:, 3);
end

%figure
plot(ConvertedData(:, 1), ConvertedData(:, 2), 'b')
hold on
plot(ConvertedData(:, 3), ConvertedData(:, 4), 'r')
```

AnalyzeForceCurveAFMWorkshop.m

```
function [AvgE, StdE, Hyster, Eptbypt] =
AnalyzeForceCurveAFMWorkshop(ConvertedData, Rtip)
IndentDepth = ConvertedData(:, 1)*10^-9; % indentation depth in m
IndentForce = ConvertedData(:, 2)*10^-9; % indentation force in N
Rtip = Rtip*10^-9; % tip radius in m
```

```
mu = 0.45; % Poisson's ratio
NumPts = length(IndentDepth);
% Indentation depth over which you will calculate the average modulus
MaxDepth = 1000*10^-9;
MinDepth = 50*10^-9;

% Hertz model: F = 4*E/3/(1-mu^2)sqrt(R)*Depth^1.5

Eptbypt = 3/4*IndentForce.*(1-mu^2)/sqrt(Rtip)./IndentDepth.^1.5*10^-3; % Point by
point modulus in kPa

MinIndex = NumPts;
MaxIndex = 1;
AreaIndent = 0;
AreaRetract = 0;
for i = 2:NumPts,
   %Sum up the areas for the hysteresis calculation
   %Area under approach curve
   if IndentDepth(i)> 0,
      AreaIndent = AreaIndent+ ConvertedData(i, 2)*(ConvertedData(i, 1)-
ConvertedData(i-1, 1));
   end
```

```
    % Area under retraction curve
    if ConvertedData(i, 3)>0,
        AreaRetract= AreaRetract+ ConvertedData(i, 4)*(ConvertedData(i, 3)-
ConvertedData(i-1, 3));
    end
    % Find the min an max indices that correspond to the region of the
    % indentation curve over which you will average the modulus
    if IndentDepth(i)>MaxDepth
        MaxIndex = i;
    elseif (IndentDepth(i) > MinDepth)
        MinIndex = i;
    end
end
MinIndex
MaxIndex
AvgE = mean(Eptbypt(MaxIndex:MinIndex));
StdE = std(Eptbypt(MaxIndex:MinIndex));
Hyster = (AreaIndent-AreaRetract)/AreaRetract; %normalized hysteresis
```

AverageModuli.m

```
function [AvgE, StdE, Moduli, AvgH, StdH, HysteresisAll] =
AverageModuli(DataStructure)
```

```
[NumFields, NumDataFiles] = size(DataStructure);
Moduli = [];
HysteresisAll = [];
for i = 1:NumDataFiles
    Moduli = [Moduli; DataStructure(i).Modulus];
    HysteresisAll = [HysteresisAll; DataStructure(i).Hysterisis];
end
AvgE = mean(Moduli);
StdE = std(Moduli);
AvgH = mean(HysteresisAll);
StdH = std(HysteresisAll);
```

SaderMethod.m

```
function SpringConstant = SaderMethod(LengthCantilever, WidthCantilever,PeakF,
varargin)
NumArg = length(varargin);
if NumArg>0 && NumArg<4,
    if NumArg == 1,
        Q = cell2mat(varargin(1));
        disp('assuming the measurements were made in air')
        air = 1;
    elseif NumArg ==2,
```

```
        if cell2mat(varargin(2)) ~=1 && cell2mat(varargin(2))~=2,
            disp('assuming the measurements were made in air')
            minF = cell2mat(varargin(1));
            maxF = cell2mat(varargin(2));
            Q = abs(PeakF/ (maxF - minF)) %calculate the quality factor (absolute value there
just in case user confuses min and max frequencies)
            air =1;
        else
            air = cell2mat(varargin(2));
            Q = cell2mat(varargin(1));
        end
    elseif NumArg == 3,
        minF = cell2mat(varargin(1));
        maxF = cell2mat(varargin(2));
        Q = abs(PeakF/ (maxF - minF)) %calculate the quality factor (absolute value there
just in case user confuses min and max frequencies)
        air = cell2mat(varargin(3));
    end


    PeakW = PeakF*2*pi*1000; % convert frequency from Hertz to radians
    Width = WidthCantilever *10^-6; % convert to m
    Length = LengthCantilever *10^-6; %convert to m
```

```
% assign fluid density (if air or water)
if air
    rho = 1.225; %kg/m3 density of air
    eta = 1.86*10^-5; %viscosity of air
else
    rho = 999.97; %kg/m3 density of water
    eta = 8.94*10^-4; %viscosity of water
end

Ren = rho*PeakW*Width^2/4/eta;

tau = log10(Ren);

OmegaR = (0.91324-0.48274*tau+0.46842*tau^2-0.12886*tau^3+0.044055*tau^4-
0.0035117*tau^5+0.00069085*tau^6)/(1-0.56964*tau+0.48690*tau^2-
0.1344*tau^3+0.045155*tau^4-0.0035862*tau^5+0.00069085*tau^6);
OmegaI = (-0.024134-0.029256*tau+0.016294*tau^2-
0.00010961*tau^3+0.000064577*tau^4-0.000044510*tau^5)/(1-
0.059702*tau+0.55182*tau^2-0.18357*tau^3+0.079156*tau^4-
0.014369*tau^5+0.0028361*tau^6);
```

```
    i = sqrt(-1);
    LambdaCirc = 1+ 4*i*besselk(1, -i*sqrt(i*Ren))/(sqrt(i*Ren)*besselk(0, -
i*sqrt(i*Ren)));
    Lambdarect = (OmegaR + OmegaI*i)*LambdaCirc;
    ImaginaryLambda = imag(Lambdarect);

    SpringConstant = 0.1906*rho*Width^2*Length*Q*PeakW^2*ImaginaryLambda;

else
    disp('incorrect number of arguments.')
end
```